Article:
Zhang, Y, Ettelaie, R orcid.org/0000-0002-6970-4650, Binks, BP et al. (1 more author) (2021) Highly Selective Catalysis at the Liquid–Liquid Interface Microregion. ACS Catalysis, 11. pp. 1485-1494. ISSN 2155-5435

https://doi.org/10.1021/acscatal.0c04604

Supporting Information

Highly Selective Catalysis at the Liquid-Liquid Interface Micro-Region

Yabin Zhang[1], Rammile Ettelaie[2], Bernard P. Binks[3], and Hengquan Yang[1]*

[1] *School of Chemistry and Chemical Engineering, Shanxi University, Taiyuan 030006, China*

[2] *Food Colloids Group, School of Food Science and Nutrition, University of Leeds, Leeds LS2 9JT, UK*

[3] *Department of Chemistry and Biochemistry, University of Hull, Hull. HU6 7RX, UK*

*To whom correspondence should be addressed: hqyang@sxu.edu.cn

Supporting Methods

1. Chemicals

Cinnamaldehyde (98%), cinnamyl alcohol (98%), furfural (99%), 3-(2-furyl)acrolein (99%), 3-methyl-2-butenal (97%), *cis*-4-heptenal (95%), methyltrimethoxysilane [$CH_3Si(OCH_3)_3$], aminopropyltriethoxysilane [$(CH_3CH_2O)_3SiCH_2CH_2CH_2NH_2$], trimethylamine [$(C_2H_5)_3N$], TiO_2 (anatase), sodium benzenesulfonate, sodium allylsulfonate, disodium piperazine-1,4-diethanesulphonate, disodium butane-1,4-disulfonate and $NaBH_4$ were purchased from the Aladdin Company (China). $RuCl_3 \cdot 3H_2O$ was purchased from Meryer Chemical Co., Ltd. (China). 4-Methoxycinnamaldehyde (97%), 4-fluorocinnamaldehyde (95%) and tri(sodiumphenylsulfonate)phosphine (TPPTS) were purchased from TCI (Shanghai) Development Co., Ltd. (E)-3-(p-Tolyl)acrylaldehyde (95%) and 4-chlorocinnamaldehyde (96%) were purchased from Adamas Reagent Co., Ltd. (China). *trans*-2-Hexenal (98%) was purchased from Alfa Aesar. Fluorescein isothiocyanate isomer I (FITC-I) was obtained from Santa Cruz Biotechnology. Water used in this study was deionized water. Unless otherwise stated, all solvents and chemicals used were of commercially available analytical grade and used without further treatment.

2. Material Synthesis

Preparation of silica (SiO_2) emulsifier. Silica nanospheres were prepared *via* an improved Stöber method.[1] 1.0 g silica nanospheres (dried at 120 °C for 4 h) was dispersed into 10 mL toluene. The suspension was subjected to sonication for 20 min. Then 4 mmol $CH_3Si(OCH_3)_3$ and 4 mmol $(C_2H_5)_3N$ were added into this suspension. After refluxing for 4 h under a N_2 atmosphere, the mixture was centrifuged. The collected solid particles were washed four times with toluene. These were dried under vacuum, thus leading to the desired methyl-modified silica (SiO_2-C).[2]

Preparation of FITC-I-labelled TNTs, FITC-I-labelled TNTs-C, and FITC-I-labelled TNTs-C^+. 1.0 g titanate nanotubes (TNTs) (dried at 120 °C for 4 h) was dispersed into toluene (8 mL). A mixture of 0.2 mmol $(CH_3CH_2O)_3SiCH_2CH_2CH_2NH_2$ (for covalent linkage with fluorescein FITC-I), 5 mmol $CH_3Si(OCH_3)_3$ and 5 mmol $(C_2H_5)_3N$ were added to this suspension. After refluxing for 4 h under a N_2 atmosphere, the mixture was isolated by centrifugation. The product was washed four times with toluene and then dried. Then 1.0 g "as-synthesized" materials and 0.001 g fluorescein isothiocyanate

isomer I (FITC-I) were dispersed into 50 mL ethanol. The mixture was stirred overnight at room temperature in the dark. After centrifuging and being washed four times with ethanol, the sample was dried. FITC-I-labelled TNTs-C was eventually obtained at the end of this procedure.[3] For FITC-I-labelled TNTs-C^+, 10 mmol $CH_3Si(OCH_3)_3$, 0.2 mmol $(CH_3CH_2O)_3SiCH_2CH_2CH_2NH_2$, 10 mmol $(C_2H_5)_3N$ were used; for FITC-I-labelled TNTs, only 0.2 mmol $(CH_3CH_2O)_3SiCH_2CH_2CH_2NH_2$ was used to modify TNTs; other procedures are all the same as that for FITC-I-labelled TNTs-C.

Preparation of Ru@TNTs, Ru@TNTs-C, and Ru@TNTs-C^+ catalysts. 1.0 g TNT materials (TNTs, TNTs-C or TNTs-C^+) was added into 40 mL acetone solution containing 0.05 g $RuCl_3 \cdot 3H_2O$ under vigorous stirring for 10 min, followed by ultrasonication for further 1 h. The suspension thus obtained was dried by rotary evaporator at 35 ºC. This was then further dried at 80 ºC for 5 h. For TNTs, the final solid was added into $NaBH_4$ aqueous solution (40 mL; 7.5 mg mL^{-1}), again vigorously stirred and aged for 30 min[4]. For TNTs-C and TNTs-C^+, the final solid was reduced with $NaBH_4$ dissolved in 40 mL of a mixture, consisting of toluene and ethanol (20:1 v/v) and aged for 30 min. The resulting suspension was centrifuged, washed with an ethanol-water solution, and finally dried in a vacuum oven at 60 ºC for 12 h. The resultant catalysts are referred to as Ru@TNTs, Ru@TNTs-C, and Ru@TNTs-C^+ respectively depending on the use of materials.

Preparation of Ru/TNTs catalyst. 1.0 g TNTs and 0.05 g $RuCl_3 \cdot 3H_2O$ were gradually added into $NaBH_4$ aqueous solution (40 mL; 7.5 mg mL^{-1}) and vigorously stirred for 30 min. The resulting suspension was centrifuged, washed with an ethanol-water solution and finally dried in a vacuum oven at 60 ºC for 12 h. The resultant catalyst is referred to as the outer surface supported catalyst Ru/TNTs.

3. Hydrogenation in conventional biphasic system

A mixture of 2.5 mL deionized water and 2.5 mL toluene was loaded in a vessel (10 mL), and the vessel was placed in a 100 mL autoclave. Before reaction, the autoclave was sealed and flushed with H_2 three times in order to remove any air. Afterwards the autoclave was charged with H_2 at a pressure of 3.0 MPa at room temperature. The sample was heated to 60 ºC within 20 min and was kept at this temperature while being stirred (700 rpm). The reaction process and conditions were the same as those in the Pickering emulsion systems. The analysis procedure was the same as that used in the Pickering emulsion reaction systems.

4. Characterization

Transmission electron microscopy (TEM) images were obtained using a JEOL-JEM-2000EX instrument. Samples for TEM observations were prepared by dispersing the sample powder in ethanol using ultrasound and then allowing a drop of the suspension to evaporate on a copper gird covered with a holey carbon film. Nitrogen-sorption measurements of titanate nanotubes (TNTs) were performed at −196 ºC on a Micromeritics ASAP 2020 analyzer. Before any measurements were taken, all samples were degassed at 120 ºC under vacuum for 6 h. The surface area was calculated from the adsorption branch in the relative pressure range of 0.05−0.15 using the Brunauer-Emmett-Teller (BET) method. X-ray photoelectron spectroscopy (XPS) was performed under an ultrahigh vacuum using a Kratos AXIS ULTRA DLD spectrometer, with Al Kα radiation and a multichannel detector. X-ray diffraction (XRD) was performed using a Bruker D2 diffractometer with Cu Kα radiation (λ = 0.15406 nm) at 40 kV and 40 mA. Thermogravimetric (TG) analysis was performed under an air atmosphere with a heating rate of 10 ºC min^{-1} using a SDT Q600 thermogravimetric analyzer. FT-IR spectra were collected with a Bruker Tensor II spectrometer in the range 400−4000 cm^{-1}. The metal content was determined by an Agilent 720ES inductively coupled plasma optical emission spectrometer (ICP-OES). ^{31}P MAS NMR was carried out at 14.1 T on a Agilent DSX-300 spectrometer with a ^{31}P frequency of 600 MHz. The dynamic interfacial tension was obtained using a DCAT21 tensiometer (Dataphysics Company, Germany) using a Wilhelmy plate. The contact angles for water on titanate nanotubes disks in air were measured using a Krüss DSA100 instrument. Before the measurement, the powder sample was compressed into a disk of thickness approximately 1 mm (*ca*. 2 MPa). A drop of water (1 μL) was injected on top of the sample disk. The appearance of the water drop was recorded at *ca*. 0.1 s with a digital camera. The value of contact angle was determined by using a photogoniometric method. Emulsion droplets were observed using an optical microscope (XSP-8CA, Shanghai, China) equipped with 10 × magnification lens. The carbon content of modified titanate nanotubes was determined on a Vario EL instrument (Elementar). Gas chromatography (GC) analysis was carried out on an Agilent 7890A analyzer (HP-5, Agilent) with a flame ionization detector. The identification of reaction products by MS spectra was performed using GC-MS (7890B-5977A, HP-5, Agilent). Confocal laser scanning microscopy images were obtained with a Carl Zeiss LSM880 instrument (Germany). The concentration of Nile red in toluene was 2×10^{-6} M, with its excitation wavelength at 559 nm.

Supporting Tables

Table S1. Results of cinnamaldehyde (CAL) hydrogenation over different catalysts in a water-ethanol system.[a]

Entry	Catalyst	Ru content (wt.%)[b]	Conversion (%)	Selectivity (%)
1	Ru@TNTs	1.6	97.0	75.4
2	Ru@TNTs-C	1.3	98.1	74.1
3	Ru@TNTs-C^+	1.4	93.3	67.0

[a]Reaction conditions: 1.0 mmol CAL, 0.5 mL ethanol used for improving the dispersion of catalyst in water, 2 mL water, 0.05 g catalyst, 0.03 g TPPTS, 60 °C, 3.0 MPa H_2, 700 rpm, 5 h. [b]ICP-OES results.

Table S2. Results of CAL hydrogenation in different solvents.[a]

Entry	Solvent	Conversion (%)	Selectivity (%)		
			COL	HCAL	HCOL
1	ethanol[b]	42.1	7.1	86.8	6.1
2	isopropanol[c]	25.4	7.4	85.0	7.6
3	ethyl acetate[d]	22.1	5.9	83.1	11.0

[a]Reaction conditions: 1 mmol CAL, 0.05 g Ru@TNTs catalyst, 0.03 g TPPTS, 60 °C, 3.0 MPa H_2, 700 rpm, 5 h. [b]5 mL ethanol. [c]5 mL isopropanol. [d]5 mL ethyl acetate.

Table S3. Results of CAL hydrogenation in different surface active additives.[a]

Entry	Additives	Conversion (%)	Selectivity (%)		
			COL	HCAL	HCOL
1	TPPTS	97.3	97.6	0.6	1.8
2	sodium dodecyl benzene sulfonate	73.2	0.1	87.3	12.6
3	sodium diphenylphosphinobenzene-3-sulfonate	90.1	89.7	2.0	8.3

[a]Reaction conditions: 2.5 mL water, 2.5 mL toluene, 1 mmol CAL, 0.05 g Ru@TNTs catalyst, 0.05 g TNTs-C, 0.05 mmol surface active additives, 60 °C, 3.0 MPa H_2, 700 rpm, 5 h.

Table S4. Comparison of the results of CAL hydrogenation over various catalysts.

Entry	Catalyst	T (°C)	P (MPa)	Conversion (%)	Selectivity (%)	TOF[a] (h^{-1})	Ref.
1	Ru@TNTs	60	3.0	97.3	97.6	19	This work[b]
2	$RuCl_3$/TPPTS	60	4.0	88	90	15.6	5
3	Ru/CNTs-ht	70	1.0	40	43	41.5	6
4	Ru/GO	60	1.5	50	71	12.7	7
5	Ru/MWNT	100	2.0	66	35	247	8
6	Ru/carbon nanofiber	110	4.5	60	43	64.8	9
7	Pt@UiO-66-NH_2	25	4.0	85.9	87.9	23.7	10
8	Pt_3Co@$Co(OH)_2$	70	0.5	99.6	90.3	41	11
9	Pt_3Co capped with oleylamine	25	0.15	100	92	8.7	12
10	MIL-101(Fe)@Pt@ MIL-101(Fe)[9.25]	25	3.0	94.3	97	13.3	13
11	Co_3O_4/MC	120	—	99	98	0.29	14
12	$CoGa_3$	100	2.0	99	96	1.8	15

[a]TOF is calculated from no. moles of converted CAL:(number of moles of total metal)$^{-1}$ h^{-1}.

[b]Inner interfacial reaction of a Pickering emulsion.

Discussion: Our Ru catalyst exhibits much higher COL selectivity than most reported Ru-based catalysts, and as high a selectivity as expensive Pt catalyst. Although the reported Co-based catalysts had high selectivity, their catalytic efficiency was relatively low.

Table S5. Results of CAL hydrogenation in different reaction locus.[a]

Entry	System	Conversion (%)	Selectivity (%)		
			COL	HCAL	HCOL
1	droplet interior reaction[b]	88.9	80.4	3.5	16.1
2	inner interfacial layer reaction[c]	97.3	97.6	0.6	1.8

[a]Reaction conditions: 2.5 mL water, 2.5 mL toluene, 1 mmol CAL, 0.05 g Ru@TNTs catalyst, 0.03 g TPPTS, 60 °C, 3.0 MPa H_2, 700 rpm, 5 h. [b]0.05 g SiO_2-C. [c]0.05 g TNTs-C.

Table S6. Results of CAL hydrogenation in different systems.[a]

Entry	Ligand	System	Conversion (%)	Selectivity (%)		
				COL	HCAL	HCOL
1	Adding disodium butane-1,4-disulfonate[b]	inner interfacial layer reaction[c]	50.0	10.0	83.2	6.8
2	Without addition of disodium butane-1,4-disulfonate	droplet interior reaction[c]	36.5	0.8	91.4	7.8
3	Adding disodium butane-1,4-disulfonate [b]	single aqueous phase reaction[d]	55.3	19.5	67.9	12.6
4	Without addition of disodium butane-1,4-disulfonate	single aqueous phase reaction[d]	55.2	18.0	68.0	14.0

[a]Reaction conditions: 1 mmol CAL, 0.05 g Ru@TNTs catalyst, 60 °C, 3.0 MPa H_2, 700 rpm, 5 h. [b]0.014 g disodium butane-1,4-disulfonate. [c]0.05 g TNTs-C, 2.5 mL water, 2.5 mL toluene. [d]5.0 mL water.

Discussion: In the inner interfacial layer reaction (in the presence of disodium butane-1,4-disulfonate that bridges TNTs-C and Ru@TNTs), the COL selectivity was improved up to 10.0% compared with the droplet interior reaction (0.8% COL selectivity in the case of the absence of disodium butane-1,4-disulfonate). Notably, disodium butane-1,4-disulfonate itself has no effect on the COL selectivity (comparing entries 3 and 4). These results further confirm that the inner interfacial layer reaction strategy is a key factor for promoting COL selectivity.

Supporting Figures

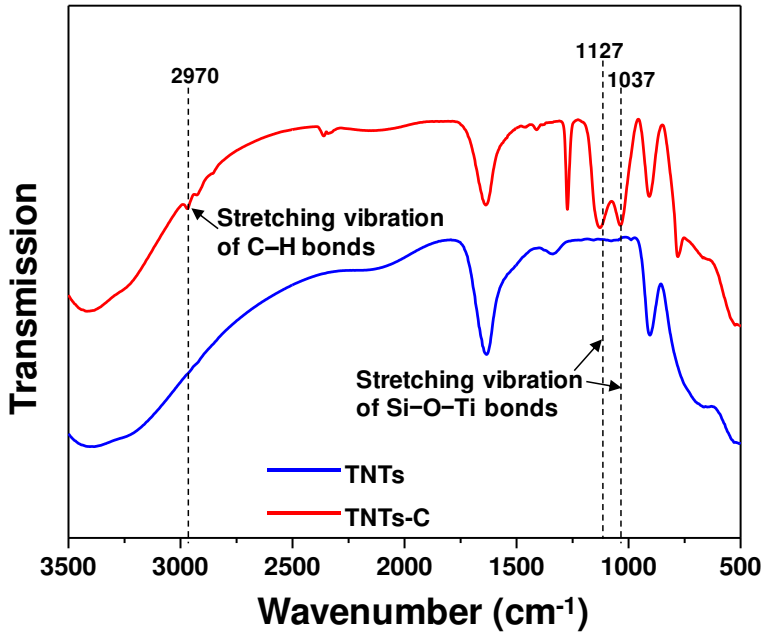

Figure S1. FT-IR spectra of TNTs and TNTs-C.

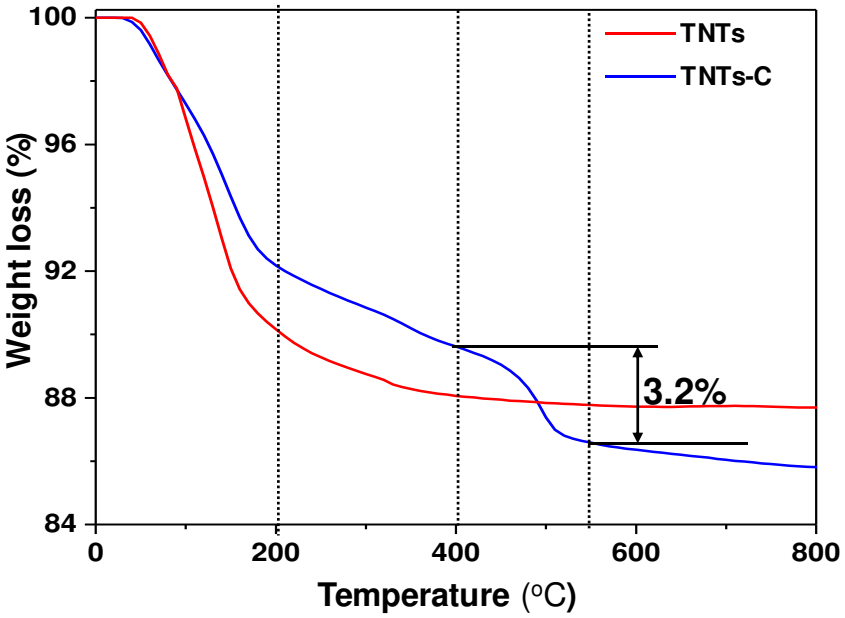

Figure S2. TG curves of TNTs and TNTs-C. The TG analyses were performed under air with a heating rate of 10 °C min^{-1}.

Discussion: Compared with TNTs, the obvious weight loss of TNTs-C occurs in the range of 400–550 °C, which is mainly related to the decomposition of methyl groups. According to the TG results, the methyl loading was estimated to be about 0.51 mmol g^{-1}, which is entirely consistent with the result determined by elemental analysis (0.51 mmol g^{-1}).

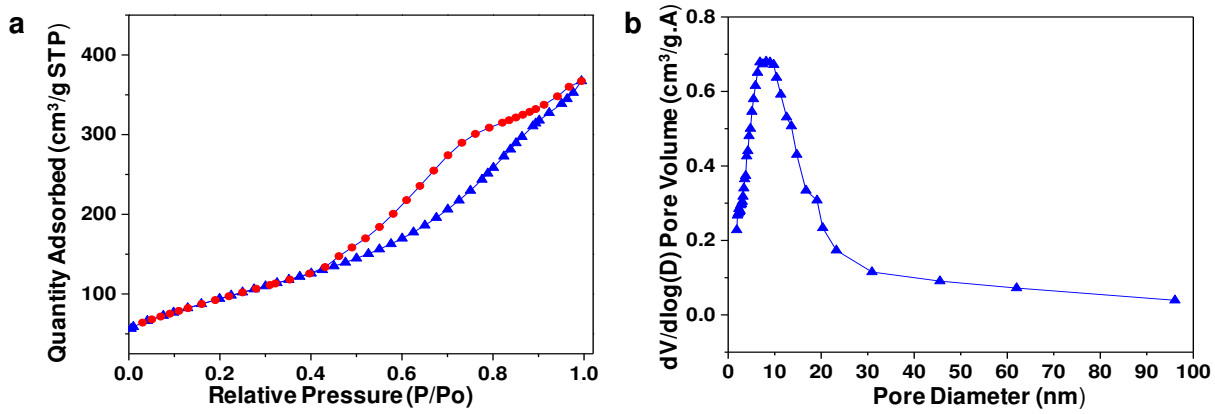

c Specific surface area, pore volume and pore size

S_{BET} (m^2 g^{-1})	V (cm^3 g^{-1})	Pore size (nm)
335	0.58	6.7

Figure S3. Results of N_2 sorption analysis of TNTs. (a) N_2 adsorption-desorption isotherms, (b) pore size distribution, (c) specific surface area, pore volume and pore size.

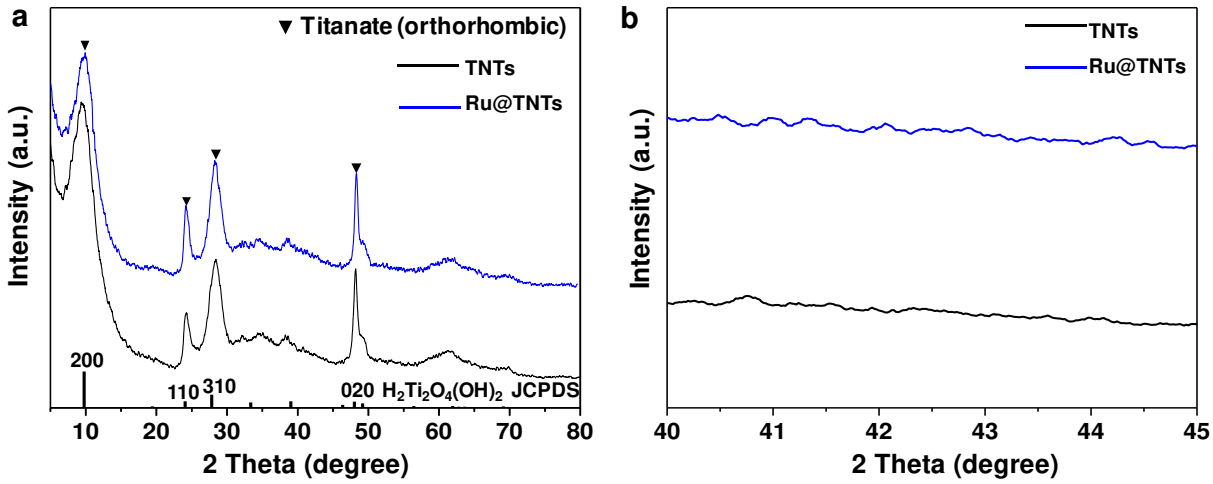

Figure S4. Powder XRD patterns. (a) Wide-range XRD patterns of TNTs, Ru@TNTs and (b) magnified patterns between 40 and 45°.

Discussion: For the bare TNTs, typical (200), (110), (310), (020) reflections at 10°, 24°, 28°, 48° were observed, which can be indexed to body-centered orthorhombic titanate (JCPDS no. 47-0124). Compared with the TNTs, the sample of Ru@TNTs displays a similar titanate phase. For Ru@TNTs, almost no reflection peak (Ru nanoparticles phase at 42–44°) was observed in the magnified pattern, implying a very high dispersion of Ru.

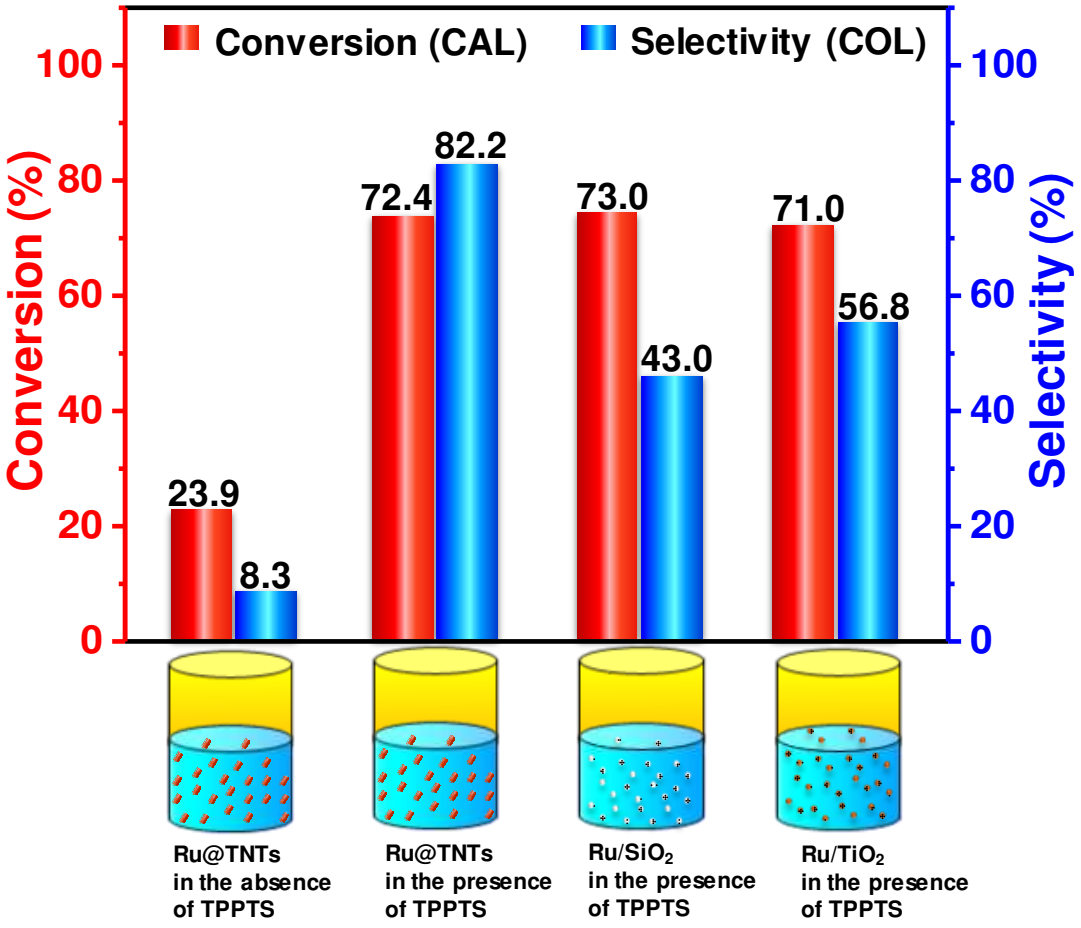

Figure S5. CAL conversion and COL selectivity over various Ru-based catalysts in water-toluene biphasic systems in the absence or presence of TPPTS. Reaction conditions: 1.0 mmol CAL, 2.5 mL toluene, 2.5 mL water, 0.05 g Ru-based catalyst if present, 0.03 g TPPTS if needed, 60 °C, 3.0 MPa H_2, 700 rpm, 5 h.

Discussion: The Ru@TNTs particles are distributed in the aqueous phase because of their high hydrophilicity, while CAL is oil-soluble. Therefore, CAL hydrogenation takes place at the oil-water interface.

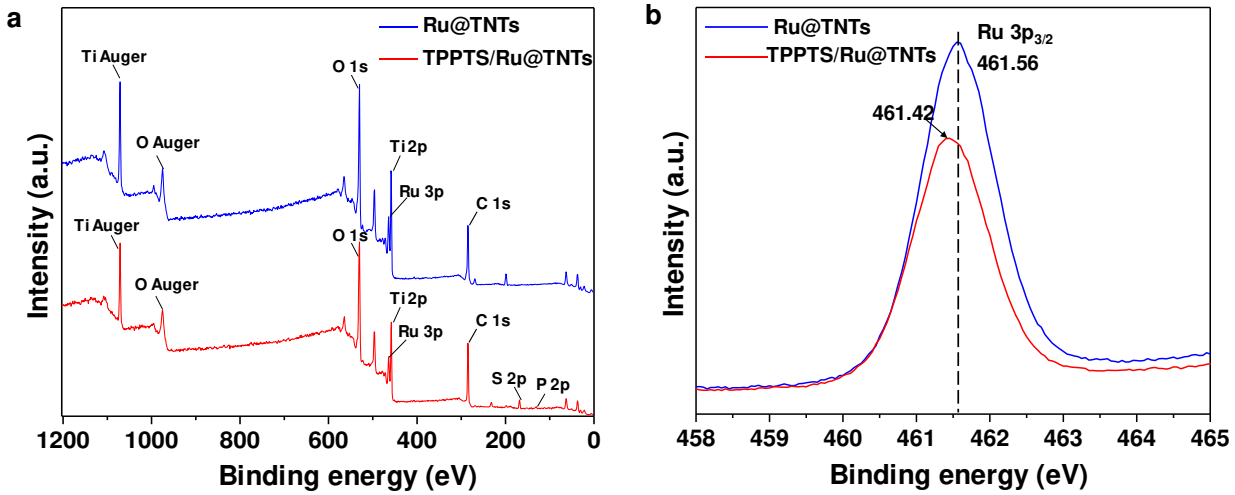

Figure S6. (a) XPS spectra and (b) Ru 3p XPS spectra of Ru@TNTs and Ru@TNTs after treatment with TPPTS solution.

Discussion: S and P elements are found in the spectrum of TPPTS/Ru@TNTs, indicating that TPPTS is adsorbed on the Ru@TNTs. Moreover, the Ru 3p binding energy for TPPTS/Ru@TNTs shows a shift (-0.14 eV) relative to that of Ru on TNTs, indicating electron donation from P to Ru.

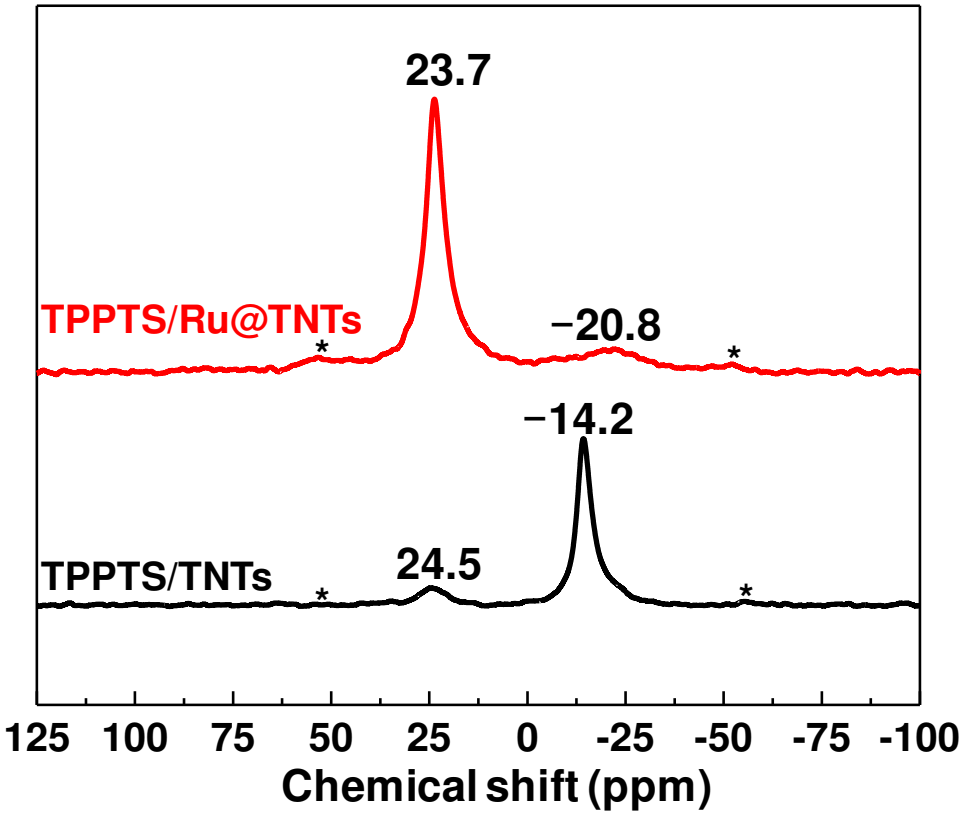

Figure S7. ^{31}P MAS NMR spectra of TPPTS/TNTs and TPPTS/Ru@TNTs (*indicates spinning sidebands).

Discussion: The ^{31}P chemical shift for free TPPTS（in solution）is –5.5 ppm (reported in previous literature)[16]. For TPPTS/TNTs, the ^{31}P chemical shift was observed to be at –14.2 ppm, which is due to the interactions of TPPTS with TNTs through coordination of -SO_3^- groups with Ti (the signal at 24.5 ppm is possibly assigned to the chemical shift of P^{5+} of TPPTS oxide adsorbed on TNTs, which was formed due to the oxidation of P^{3+} of TPPTS but exists in a small fraction[17]). For TPPTS/Ru@TNTs, the ^{31}P chemical shift was found to be at 23.7 ppm, indicating the strong coordination between the Ru metal nanoparticle and P.

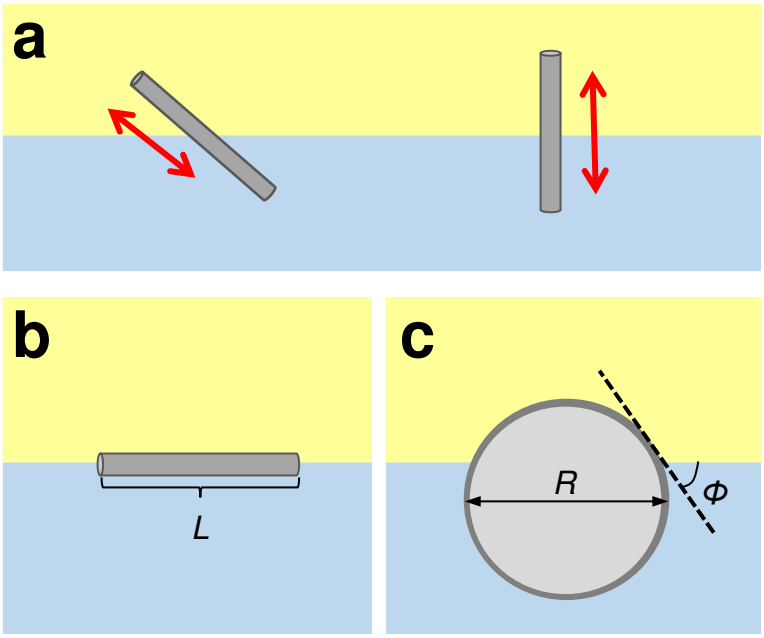

Figure S8. Possible orientations of a nanotube at the oil-water interface. (a) Tilted and upright nanotubes, (b) nanotube lying flat, (c) cross-sectional view of the tilted nanotube.

Discussion: The orientation of a nanotube (*n*) at the oil (*o*)-water (*w*) interface is dictated by consideration of the surface energies arising from three distinct interfaces; that between nanotube and water, between nanotube and oil and finally the one between oil and water. In general the equilibrium position and orientation will turn out to be the one that minimizes the total sum of these three energies (*E*), namely

$$E = \gamma_{n-w}A_{n-w} + \gamma_{n-o}A_{n-o} + \gamma_{o-w}A_{o-w} \qquad (1)$$

where $A_{n\text{-}w}$ is the area of contact between the nanotube and water, while $\gamma_{n\text{-}w}$ represents the corresponding interfacial tension (energy per unit area) at the same interface. Symbols A and γ with different suffixes, *n*-*o* and *o*-*w*, represent the corresponding quantities for the interface between the nanotube and oil, and that between the oil and water phases, respectively. It is clear that orientations such as those shown in Figure S8a, where the nanotube has penetrated along its axis into both oil and water, will not be stable.

For these, it is always possible to move the nanotube up or down along their main axis such as to increase the contact between the nanotube and the more wetting fluid (*i.e.* the one with the lower

interfacial tension at nanotube surface), while leaving the oil-water contact area unchanged. So for example if $\gamma_{n\text{-}o}<\gamma_{n\text{-}w}$, then the nanotube can move further into the oil phase, increasing its contact area with oil and reducing it with water. This results in a decrease of energy. The process can continue until the nanotube is fully immersed in the oil phase. The opposite occurs if $\gamma_{n\text{-}o}>\gamma_{n\text{-}w}$ with the nanotube now fully immersed in the water phase. The only different convincable orientation which may result in minimization of E in equation (1) is the one where the nanotube is lying parallel to the oil-water surface, as is depicted in Figure S8b.

To determine the angle Φ taken by the cylindrical nanotube at the interface, as shown in Figure S8c, we express all areas appearing in equation (1) in terms of this angle. This leads to:

$$E = LR[2\gamma_{n-w}(\pi - \emptyset) + 2\gamma_{n-o}\emptyset - 2\gamma_{o-w}\sin(\emptyset)] \qquad (2)$$

where the final term involving $\sin(\Phi)$ is negative, reflecting the fact that when the nanotube is at the interface the contact area between the oil and water is reduced. In equation (2), symbols R and L stand for the outer radius and length of the nanotube, respectively. Now differentiating E with respect to angle Φ and setting this to zero yields the required equation for the angle that minimizes the energy. This yields the equilibrium position of the nanotube at the oil-water interface as:

$$\frac{\partial E}{\partial \emptyset} = 2LR(-\gamma_{n-w} + \gamma_{n-o} - \gamma_{o-w}\cos(\emptyset)) = 0 \qquad (3)$$

which in turn leads to

$$\cos(\emptyset) = \frac{\gamma_{n-o}-\gamma_{n-w}}{\gamma_{o-w}} \qquad (4)$$

Now the right-hand side of equation (4) in accordance with Young's equation is simply $\cos(\theta)$, where θ is the contact angle between water, oil and the material from which the outer wall of the nanotube is constructed. Thus the nanotubes will adopt a position on the interface such that Φ is equal to the contact angle θ for the outer walls of the nanotubes.

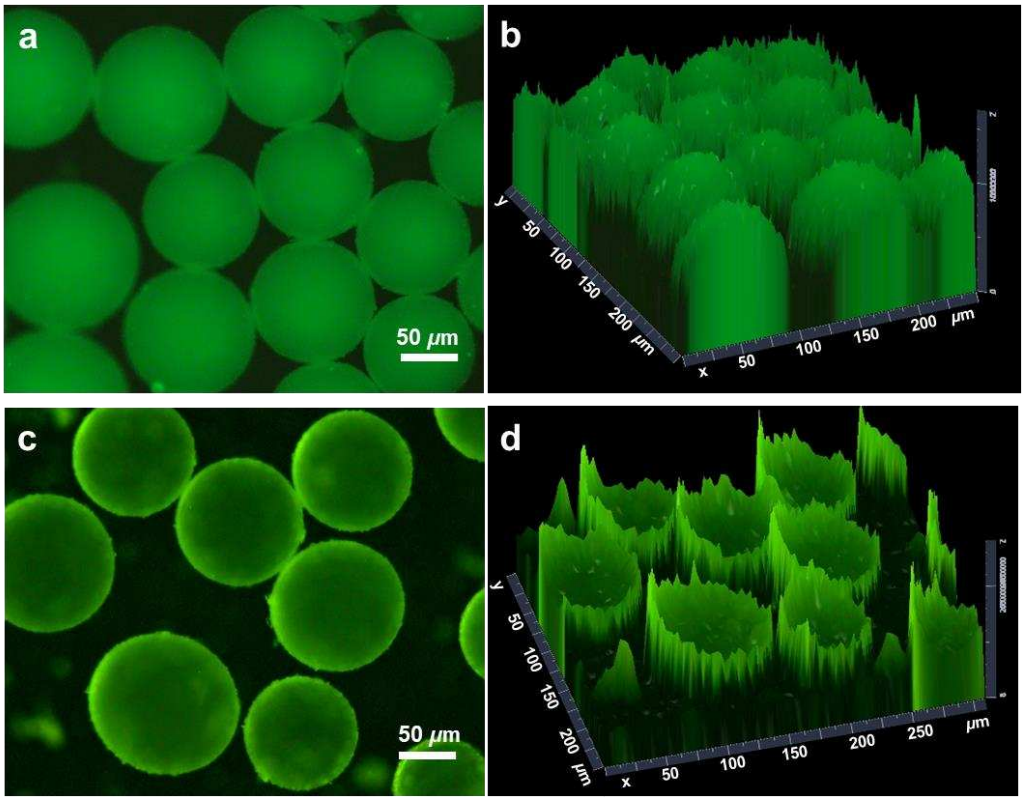

Figure S9. Fluorescence confocal microscopy images of Pickering emulsions in the absence or presence of TPPTS. (a) 2D image for the w/o emulsion in the absence of TPPTS and (b) corresponding 3D graph. (c) 2D image for the w/o emulsion in the presence of TPPTS and (d) corresponding 3D graph. The emulsion consists of 2.5 mL water, 2.5 mL toluene, 0.03 g TPPTS (for c and d), 0.05 g TNTs-C as emulsifier, 0.05 g FITC-I-labelled Ru@TNTs.

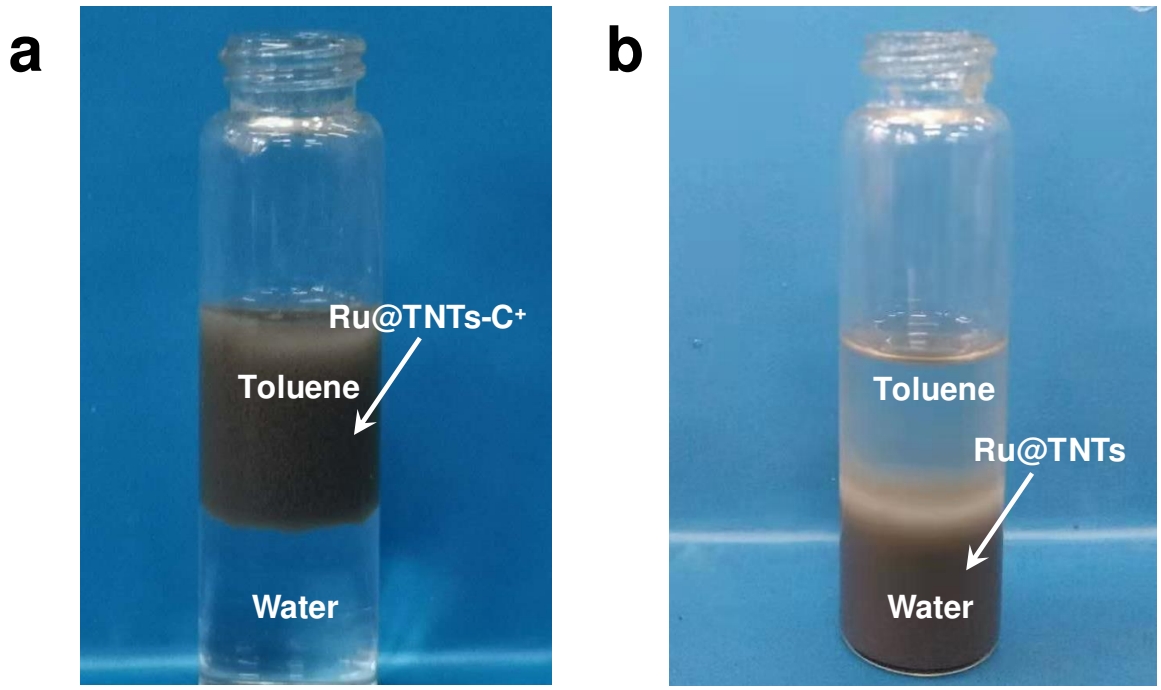

Figure S10. Distribution of (a) Ru@TNTs-C^+ and (b) Ru@TNTs in a toluene-water biphasic system after shearing.

Discussion: Ru@TNTs-C^+ particles are too hydrophobic to stabilize an emulsion, while Ru@TNTs particles are too hydrophilic to stabilize an emulsion.

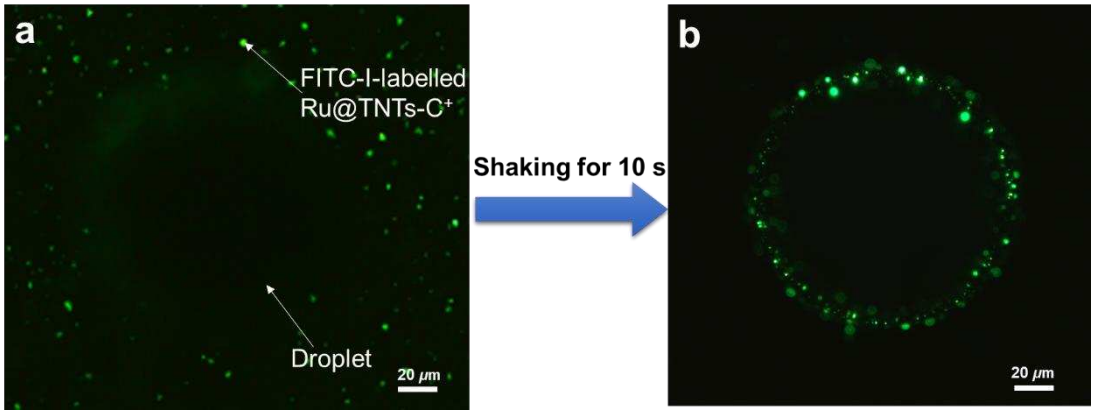

Figure S11. Fluorescence confocal microscopy images for the adsorption of Ru@TNTs-C^+ at outer interfacial layer of Pickering droplet in the absence of TPPTS. (a) FITC-I-labelled Ru@TNTs-C^+ was just dispersed into the continuous phase without shaking. (b) The FITC-I-labelled Ru@TNTs-C^+ adsorbed on the outer interface of droplet after shaking for 10 s. The emulsion consists of 2.5 mL water, 2.5 mL toluene, 0.05 g TNTs-C as emulsifier, 0.05 g FITC-I-labelled Ru@TNTs-C^+ dispersed in toluene.

Discussion: No fluorescence circles were observed when FITC-I-labelled Ru@TNTs-C^+ was just added into the continuous phase (toluene) of a w/o Pickering emulsion. However, after shaking for 10 s, the FITC-I-labelled Ru@TNTs-C^+ particles migrates to the outer interfacial layer of droplets.

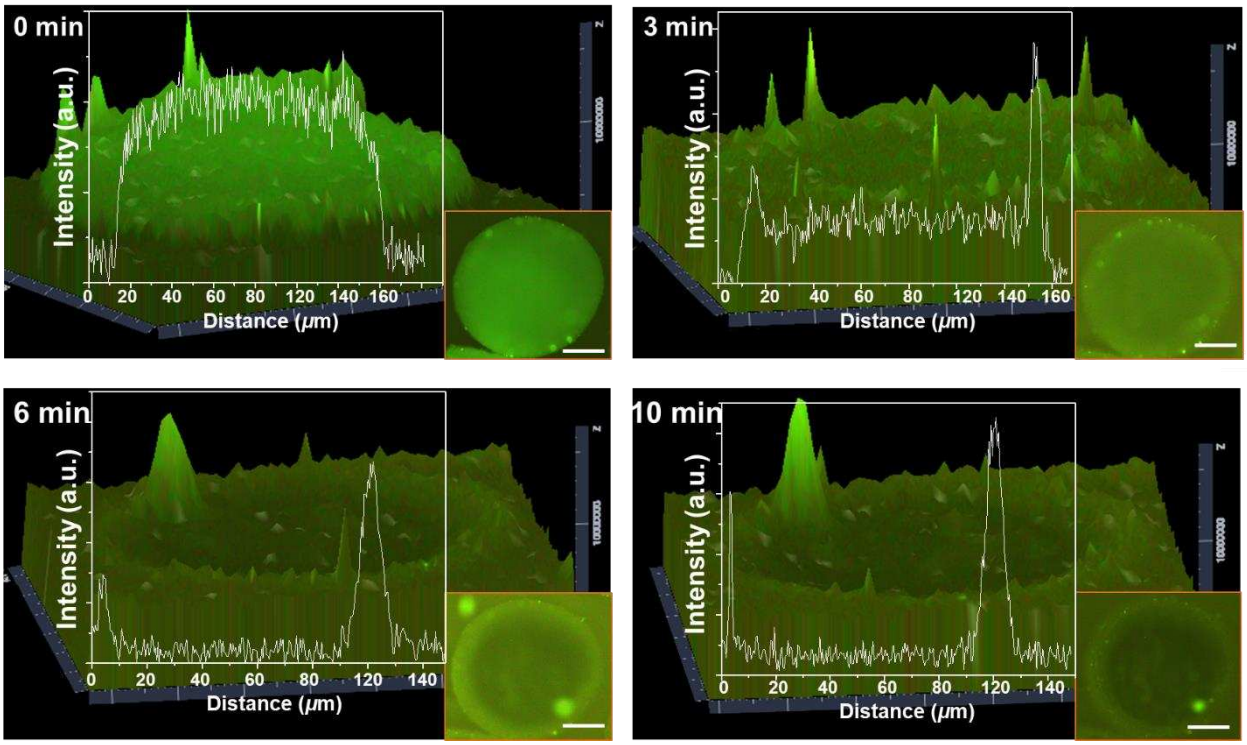

Figure S12. 3D fluorescence confocal microscopy graphs showing the migration of Ru@TNTs toward the inner interfacial layer of w/o emulsion droplet with time. The emulsion system consists of 2.5 mL water, 2.5 mL toluene, 0.03 g TPPTS, 0.05 g TNTs-C, 0.05 g FITC-I-labelled Ru@TNTs, scale bar = 50 μm.

Discussion: The fluorescence intensity at the inner interfacial layer of a droplet gradually increased and then levelled off, while the fluorescence intensity of the interior of a droplet gradually decreased and levelled off after we shook the Pickering emulsion. These observations indicate that Ru@TNTs (FITC-I-labelled) migrated from the interior of a droplet to the inner interfacial layer.

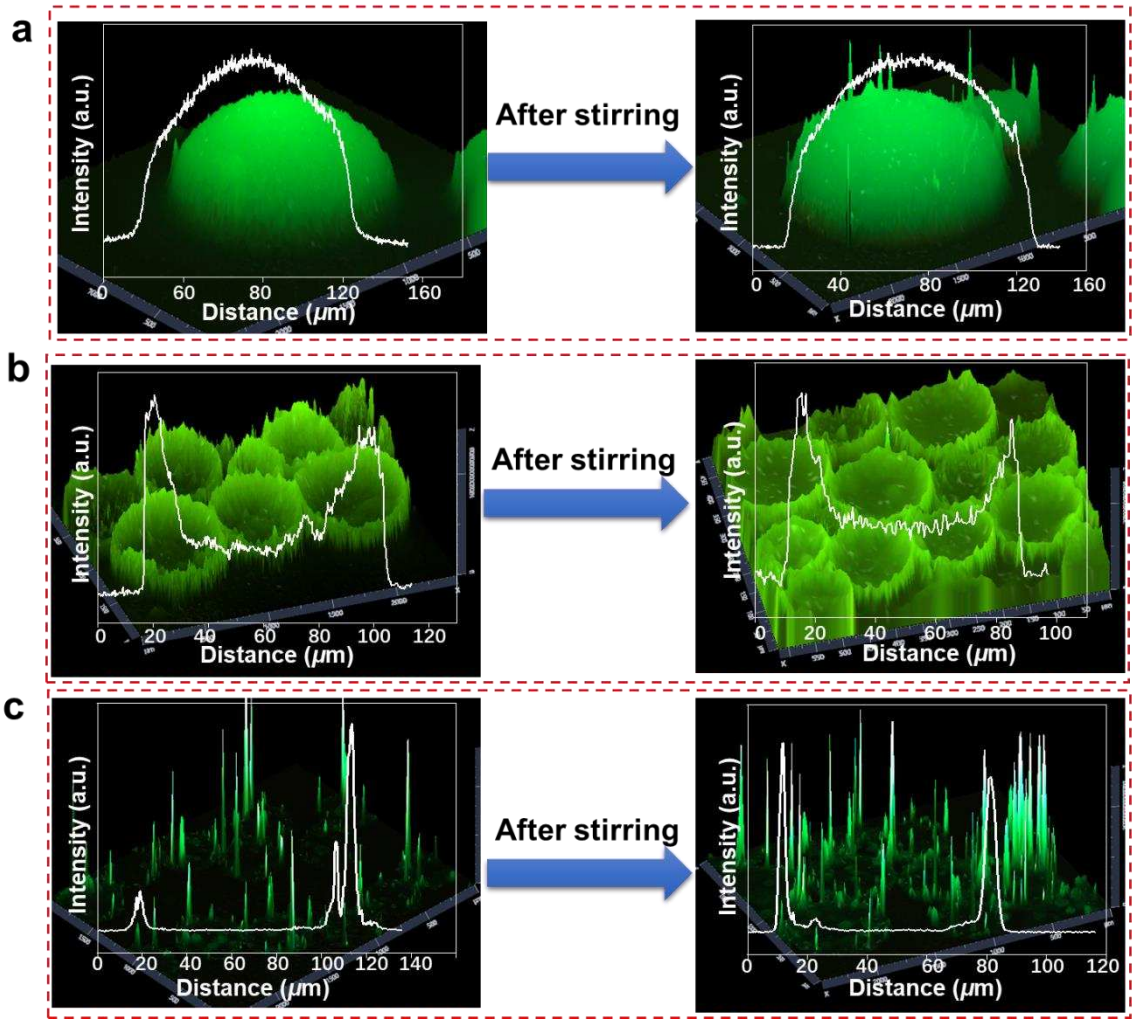

Figure S13. Fluorescence confocal microscopy images of Pickering emulsions before and after stirring (700 rpm, 1 h). (a) 3D graphs for the droplet interior reaction system. (b) 3D graphs for the inner interfacial layer reaction system. (c) 3D graphs for the outer interfacial layer reaction system. The emulsion consists of 2.5 mL water, 2.5 mL toluene, 0.03 g TPPTS (for b and c), 0.05 g TNTs-C as emulsifier, 0.05 g FITC-I-labelled Ru@TNTs (for a and b), 0.05 g FITC-I-labelled Ru@TNTs-C^{+} (for c).

Discussion: To check whether the stirring leads to the change of the catalyst location, we had employed fluorescence microscopy to observe the catalyst positions before and after stirring. As shown in Figure S13, after stirring (700 rpm, 1 h), the fluorescence intensity (the FITC-I-labelled catalysts) did not change in the droplet interior reaction system, the inner interfacial layer reaction system, and the outer interfacial layer reaction system.

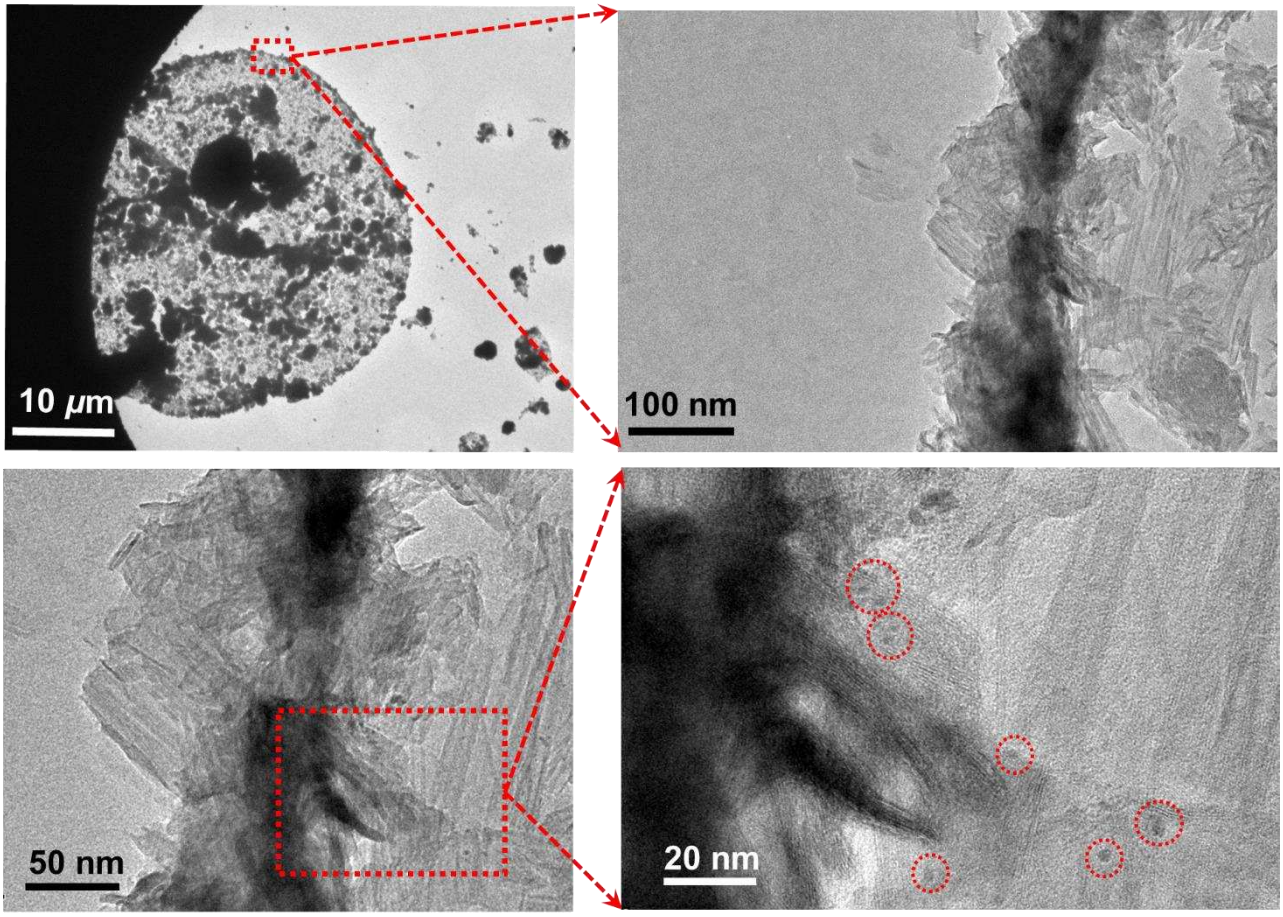

Figure S14. Cryo-TEM images of the w/o Pickering emulsion and Ru@TNTs adsorbed on the inner surface of emulsion droplet. The emulsion consists of 2.5 mL water, 2.5 mL toluene, 0.03 g TPPTS, 0.01 g solid emulsifier (TNTs-C) and 0.01 g Ru@TNTs. Cryo-TEM images were obtained using a JEOL-2100F instrument, and samples were kept at −170 ºC during the TEM observations.

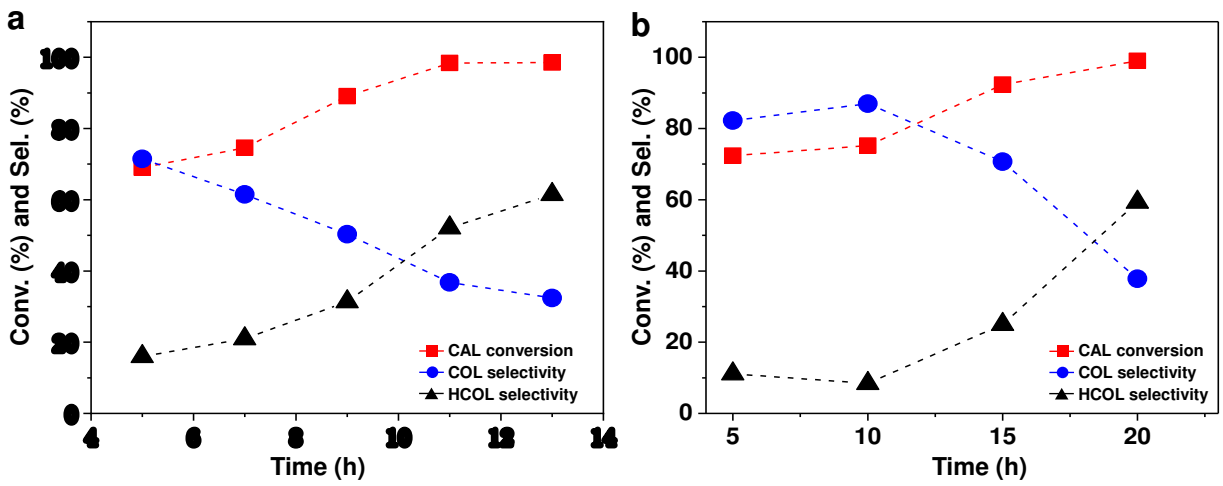

Figure S15. Conversion and selectivity of CAL hydrogenation with time, achieved over the Ru@TNTs catalyst in (a) an aqueous system and (b) water-toluene biphasic system. Reaction conditions: 0.05 g Ru@TNTs, 1.0 mmol CAL, 0.03 g TPPTS, 3.0 MPa H_2, 60 °C, 700 rpm, 5 mL water as solvent for (a), and 2.5 mL water and 2.5 mL toluene for (b).

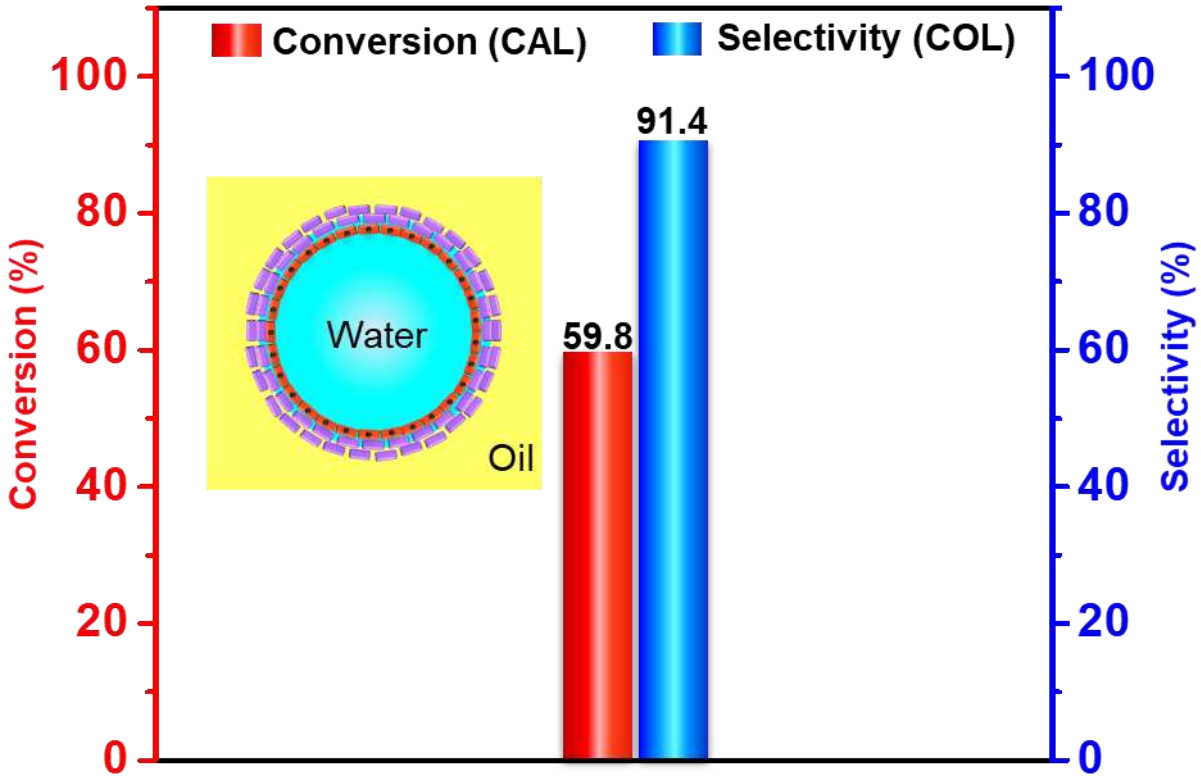

Figure S16. CAL conversion and COL selectivity in the inner interfacial layer reaction with increased droplet surface coverage. Reaction conditions: 2.5 mL water, 2.5 mL toluene, 0.1 g TNTs-C, 0.05 g Ru@TNTs, 1.0 mmol CAL, 0.03 g TPPTS, 3.0 MPa H_2, 60 °C, 700 rpm, 5 h.

Discussion: Double dose of interface-active particles (0.1 g TNTs-C) was used, while the dose of the Ru@TNTs catalyst was kept the same as the inner interfacial layer reaction system in Figure 3. By employing 3000 rpm, the droplet sizes were close to those of emulsions in Figure 3. Due to doubling the interface-active particles, the droplet surface coverage is increased. In this case the reactant had less chance to access catalyst (at inner interfacial layer), leading to a significant decrease in the CAL conversion but a slight decrease in the COL selectivity (relative to the inner interfacial layer reaction in Figure 4A).

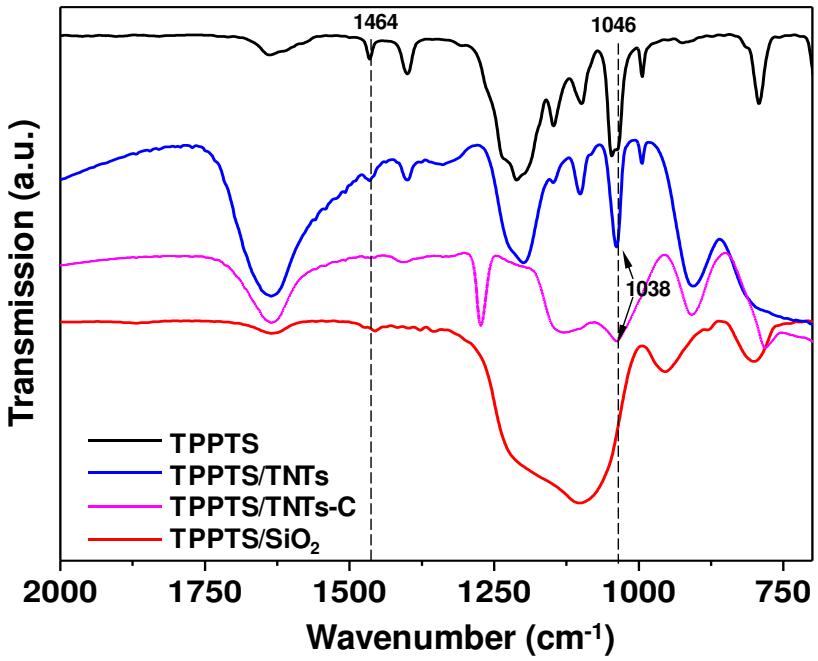

Figure S17. FT-IR spectra of TPPTS, TPPTS/TNTs, TPPTS/TNTs-C and TPPTS/SiO_2.

Discussion: The peaks at 1464 cm^{-1} and at 1046 cm^{-1} are attributed to the stretching vibration of aromatic ring and the antisymmetric stretching vibration of S-O groups in TPPTS, respectively. The appearance of these two peaks in the spectra of TNTs and TNTs-C treated with TPPTS indicates that TPPTS is adsorbed on TNTs and TNTs-C. Notably, the peak of 1046 cm^{-1} was observed to shift to 1038 cm^{-1}, implying the coordination of the S-O groups of TPPTS with surface Ti centers of TNTs and TNTs-C. As a reference, silica does not show this coordination effect.

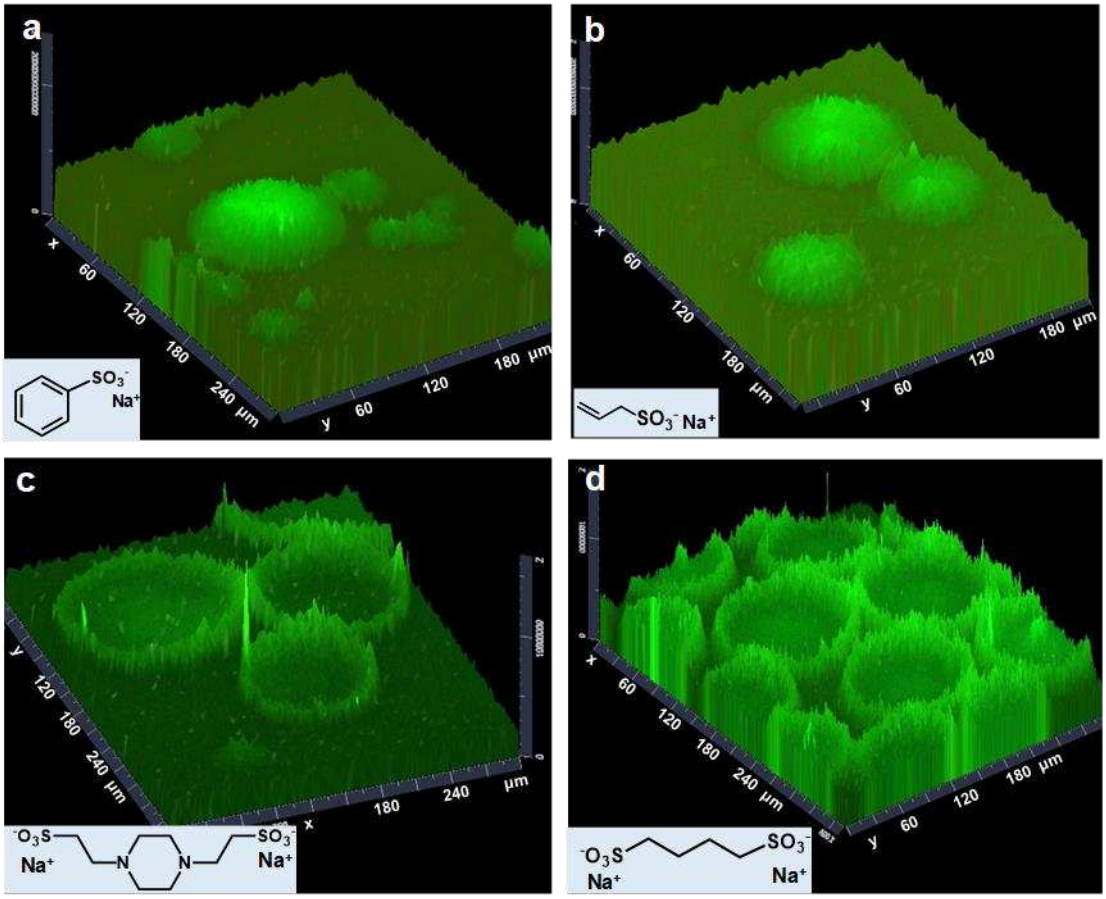

Figure S18. 3D fluorescence confocal microscopy graphs for w/o Pickering emulsions in the presence of different ligands containing SO_3^- groups. (a) sodium benzenesulfonate, (b) sodium allylsulfonate, (c) disodium piperazine-1,4-diethanesulphonate, (d) disodium butane-1,4-disulfonate. The emulsion consists of 2.5 mL water, 2.5 mL toluene, 0.05 mmol different ligands, 0.05 g TNTs-C, 0.05 g FITC-I-labelled Ru@TNTs.

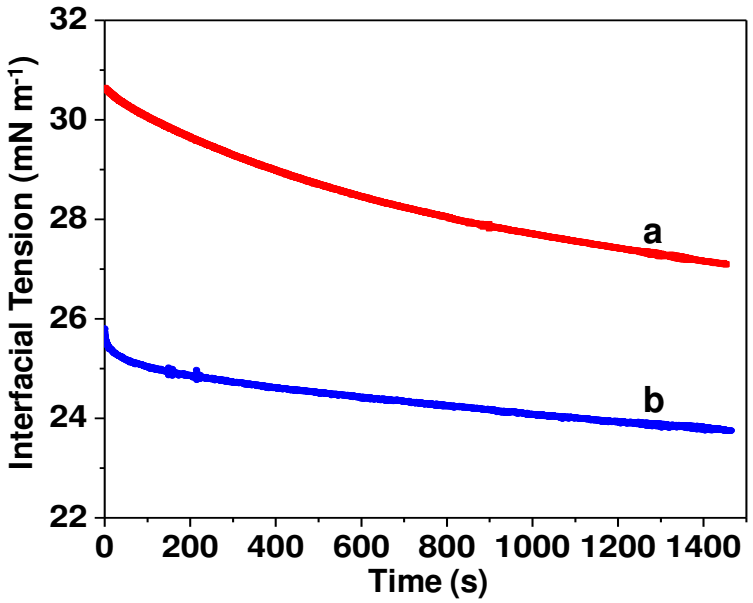

Figure S19. Dynamic interfacial tensions for different biphasic systems: (a) 3 mg mL^{-1} TPPTS in water and 5 mg mL^{-1} SiO_2-C in toluene; (b) 3 mg mL^{-1} TPPTS and 5 mg mL^{-1} Ru@TNTs in water, 5 mg mL^{-1} SiO_2-C in toluene.

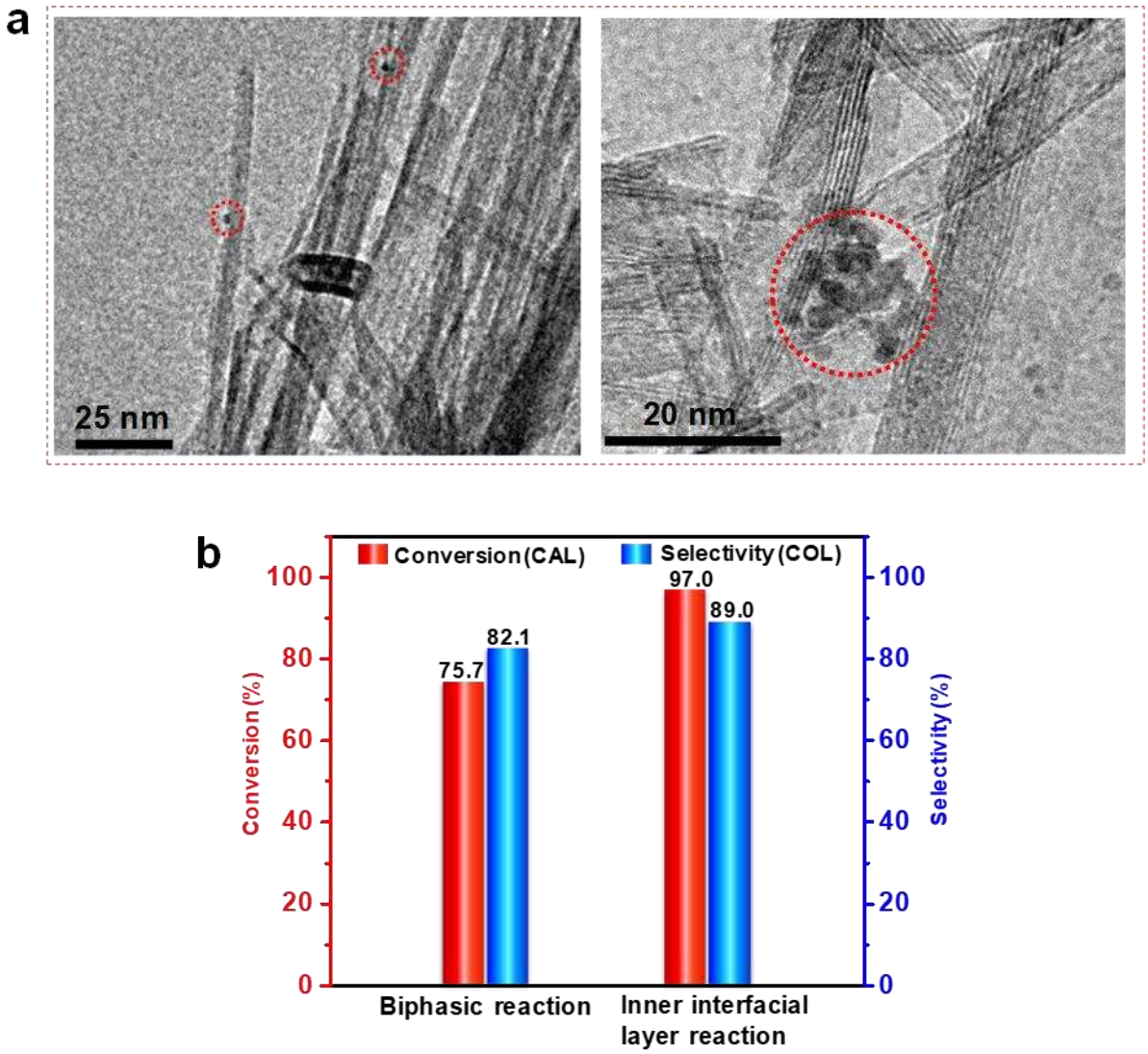

Figure S20. (a) TEM images of Ru/TNTs, in which Ru nanoparticles are located on the outer surface of TNTs. (b) Results of CAL hydrogenation over the Ru/TNTs in a water-toluene biphasic system and in the inner interfacial layer of Pickering emulsion. Reaction conditions: 0.05 g Ru/TNTs, 0.05 g TNTs-C (inner interfacial layer reaction), 0.03 g TPPTS, 1 mmol CAL, 2.5 mL toluene, 2.5 mL water, 3.0 MPa H_2, 60 °C, 700 rpm, 5 h.

Discussion: The Ru/TNTs catalyst gave CAL conversion and COL selectivity comparable to Ru@TNTs both in a water-toluene biphasic system and in the inner interfacial layer of a Pickering emulsion. This indicates that the selectivity enhancement is not due to the confinement effects caused by the nanotube space.

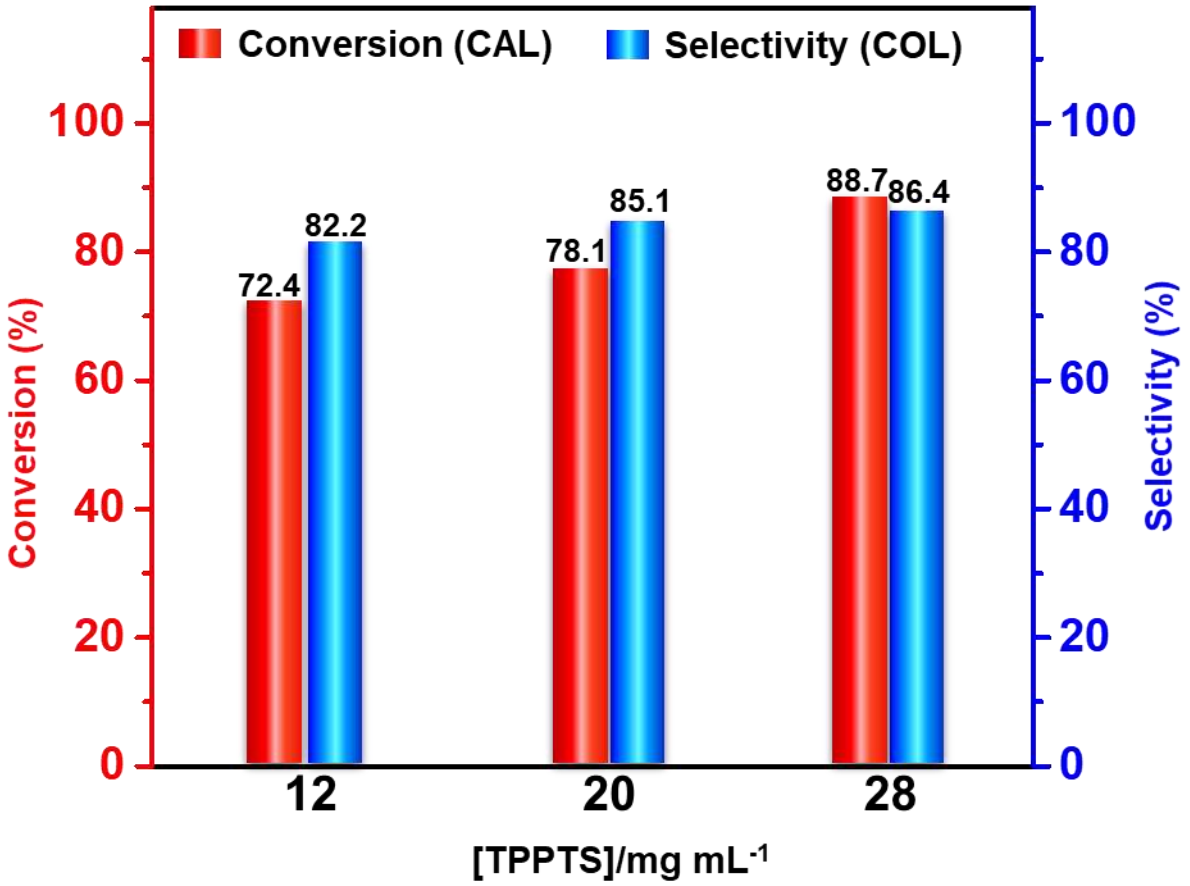

Figure S21. CAL conversion and COL selectivity in a conventional water-toluene biphasic system in the presence of different concentrations of TPPTS. Reaction conditions: 0.05 g Ru@TNTs, 1 mmol CAL, 2.5 mL toluene, 2.5 mL water, 3.0 MPa H_2, 60 °C, 700 rpm, 5 h.

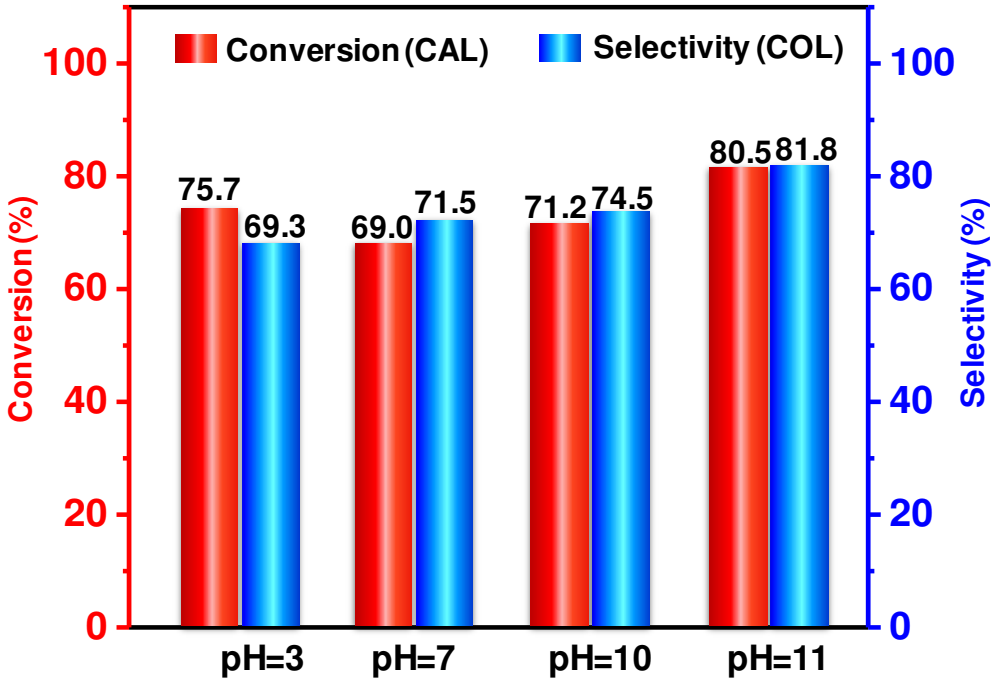

Figure S22. CAL conversion and COL selectivity in single aqueous phase system at different pHs. HCl solution (1 M) and NaOH solution (1 M) were used to adjust the pH. Reaction conditions: 0.05 g Ru@TNTs, 0.03 g TPPTS, 1 mmol CAL, 5 mL water, 3.0 MPa H_2, 60 °C, 700 rpm, 5 h.

Discussion: As the pH of the aqueous phase increases, the COL selectivity gradually increases. This is because OH^- ions inhibit the adsorption of C=C bond by electrostatically repelling the phenyl ring of cinnamaldehyde on the surface of Ru nanoparticles[18].

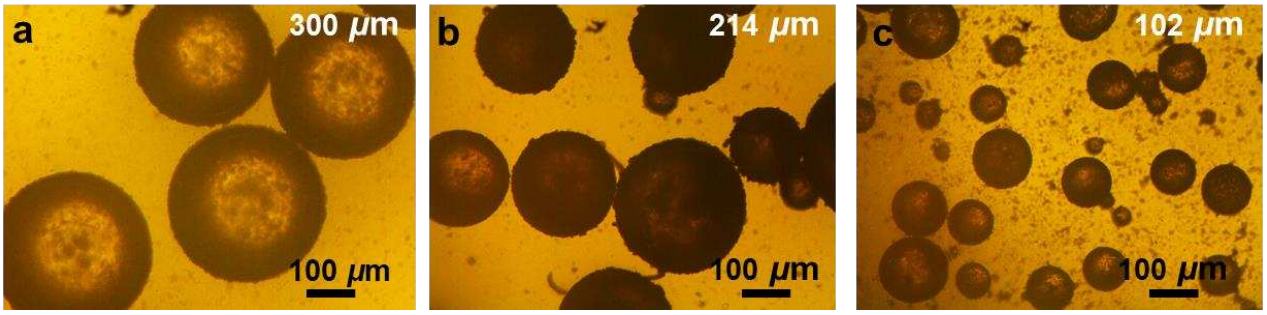

Figure S23. Optical microscopy images of w/o Pickering emulsions with different droplet diameters. Pickering emulsions were formulated using different stirring rates: (a) 1,000 rpm, (b) 5,000 rpm, (c) 10,000 rpm. The emulsion consists of 2.5 mL water, 2.5 mL toluene, 0.03 g TPPTS, 0.05 g TNTs-C, 0.05 g Ru@TNTs.

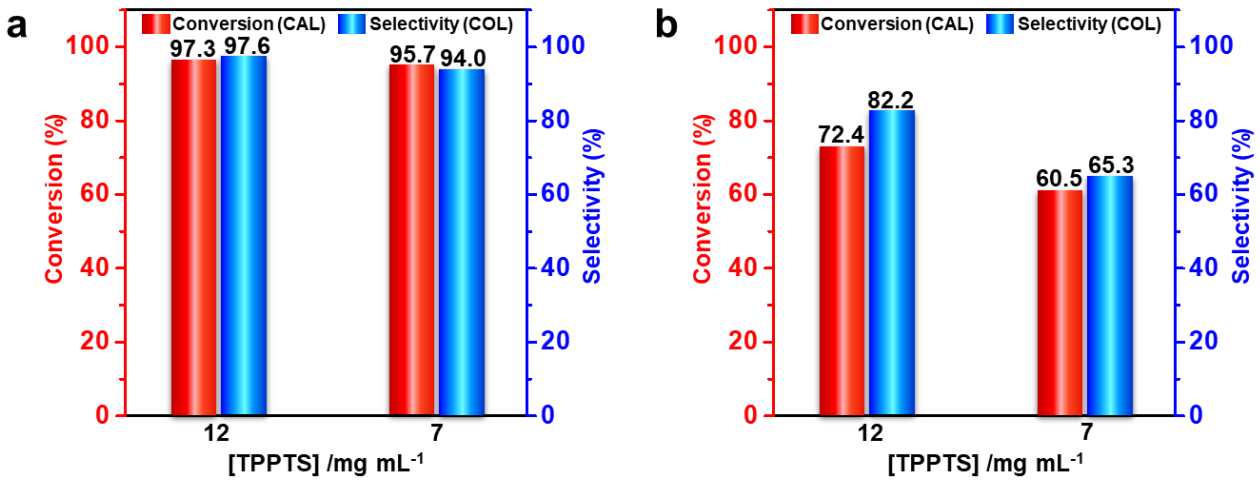

Figure S24. CAL conversion and COL selectivity in (a) the inner interfacial layer reaction systems and (b) the conventional water-toluene biphasic reaction systems in the presence of different concentrations of TPPTS. Reaction conditions: 0.05 g TNTs-C for Pickering emulsion systems, 0.05 g Ru@TNTs, 1 mmol CAL, 2.5 mL toluene, 2.5 mL water, 3.0 MPa H_2, 60 °C, 700 rpm, 5 h.

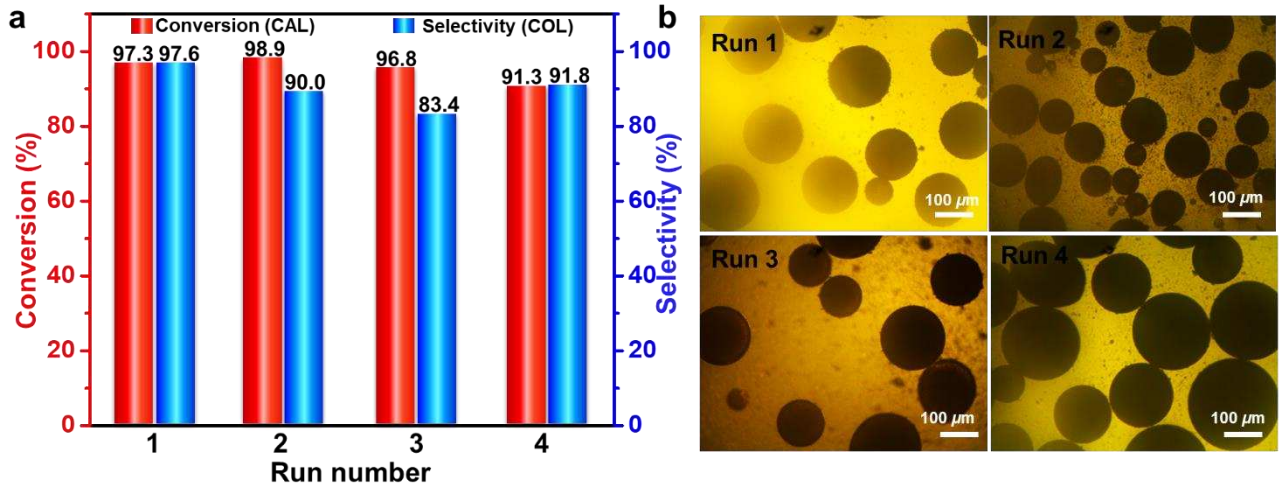

Figure S25. (a) Recycling results of the Ru@TNTs catalyst in w/o Pickering emulsions. (b) Optical microscopy images for w/o Pickering emulsions during multiple reaction cycles. Reaction conditions: 0.05 g TNTs-C, 0.05 g Ru@TNTs, 1.0 mmol CAL, 0.03 g TPPTS, 2.5 mL toluene, 2.5 mL water, 3.0 MPa H_2, 60 °C, 700 rpm, 5 h.

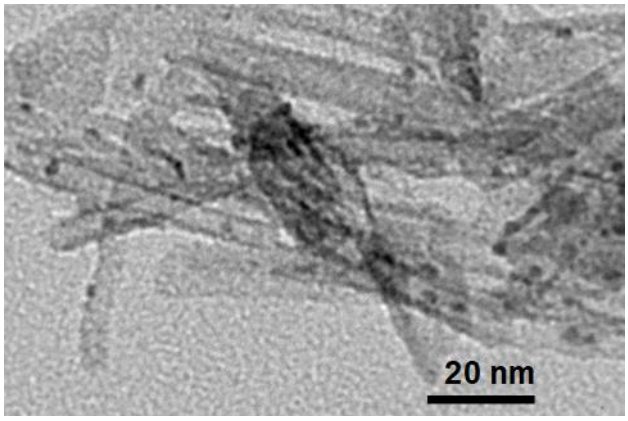

Figure S26. TEM image of Ru@TNTs after 4 reaction cycles.

Supporting References

1. Kong, D. Y.; Zhang, C. M.; Xu, Z. H.; Li, G. G.; Hou, Z. Y.; Lin, J. Tunable photoluminescence in monodisperse silica spheres. *J. Colloid Interface Sci.* **2010**, *352*, 278−284.

2. Zhang, Y. B.; Zhang, M.; Yang, H. Q. Tuning biphasic catalysis reaction with a Pickering emulsion strategy exemplified by selective hydrogenation of benzene. *ChemCatChem* **2018**, *10*, 5224−5230.

3. Zhang, M.; Ettelaie, R.; Yan, T.; Zhang, S. J.; Cheng, F. Q.; Binks, B. P.; Yang, H. Q. Ionic liquid droplet microreactor for catalysis reactions not at Equilibrium. *J. Am. Chem. Soc.* **2017**, *139*, 17387−17396.

4. Liu, J.; He, S.; Li, C. M.; Wang, F.; Wei, M.; Evans, D. G.; Duan, X. Confined synthesis of ultrafine Ru–B amorphous alloy and its catalytic behavior toward selective hydrogenation of benzene. *J. Mater. Chem. A* **2014**, *2*, 7570−7577.

5. Fujita, S. I.; Sano, Y.; Bhanage, B. M.; Arai, M. Supported liquid-phase catalysts containing ruthenium complexes for selective hydrogenation of *α,β*-unsaturated aldehyde: importance of interfaces between liquid film, solvent, and support for the control of product selectivity. *J. Catal.* **2004**, *225*, 95−104.

6. Wang, Y.; Rong, Z. M.; Wang, Y.; Zhang, P.; Wang, Y.; Qu, J. P. Ruthenium nanoparticles loaded on multiwalled carbon nanotubes for liquid-phase hydrogenation of fine chemicals: An exploration of confinement effect. *J. Catal.* **2015**, *329*, 95−106.

7. Dongil, A. B.; Bachiller-Baeza, B.; Guerrero-Ruiz, A.; Rodríguez-Ramos, I. Chemoselective hydrogenation of cinnamaldehyde: A comparison of the immobilization of Ru–phosphine complex on graphite oxide and on graphitic surfaces. *J. Catal.* **2011**, *282*, 299−309.

8. Vu, H.; Gonçalves, F.; Philippe, R.; Lamouroux, E.; Corrias, M.; Kihn, Y.; Plee, D.; Kalck, P.; Serp, P. Bimetallic catalysis on carbon nanotubes for the selective hydrogenation of cinnamaldehyde. *J. Catal.* **2006**, *240*, 18−22.

9. Toebes, M. L.; Prinsloo, F. F.; Bitter, J. H.; Dillen, A. J.; Jong, K, P. Influence of oxygen-containing surface groups on the activity and selectivity of carbon nanofiber-supported ruthenium catalysts in the hydrogenation of cinnamaldehyde. *J. Catal.* **2003**, *214*, 78−87.

10. Guo, Z. Y.; Xiao, C. X.; Maligal-Ganesh, R. V.; Zhou, L.; Goh, T. W.; Li, X. L.; Tesfagaber, D.; Thiel, A.; Huang, W. Y. Pt nanoclusters confined within metal–organic framework cavities for chemoselective cinnamaldehyde hydrogenation. *ACS Catal.* **2014**, *4*, 1340−1348.

11. Wang, H. P.; Bai, S, X.; Pi, Y. C.; Shao, Q.; Tan, Y. M.; Huang, X. Q. A Strongly coupled ultrasmall Pt_3Co nanoparticle-ultrathin $Co(OH)_2$ nanosheet architecture enhances selective hydrogenation of *α,β*-unsaturated aldehydes. *ACS Catal.* **2019**, *9*, 154−159.

12. Wu, B. H.; Huang, H. Q.; Yang, J.; Zheng, N. F.; Fu, G. Selective hydrogenation of *α,β*-unsaturated aldehydes catalyzed by amine-capped Platinum-Cobalt nanocrystals. *Angew. Chem. Int. Ed.* **2012**, *51*, 3440−3443.

13. Yuan, K.; Song, T. Q.; Wang, D. W.; Zhang, X. T.; Gao, X.; Zou, Y.; Dong, H. L.; Tang, Z. Y.; Hu, W. P. Effective and selective catalysts for cinnamaldehyde hydrogenation: hydrophobic hybrids of metal–organic frameworks, metal nanoparticles, and micro- and mesoporous polymers. *Angew. Chem. Int. Ed.* 2018, *57*, 5708−5713.

14. Wang, G. H.; Deng, X. H.; Gu, D.; Chen, K.; Tüysüz, H.; Spliethoff, B.; Bongard, H.; Weidenthaler, C.; Schmidt, W.; Schüth, F. Co_3O_4 nanoparticles supported on mesoporous carbon for selective transfer hydrogenation of *α,β*-unsaturated aldehydes. *Angew. Chem. Int. Ed*. **2016**, *55*, 11101−11105.

15. Yang, Y. S.; Rao, D. M.; Chen, Y. D.; Dong, S. Y.; Wang, B.; Zhang, X.; Wei, M. Selective hydrogenation of cinnamaldehyde over Co-based intermetallic compounds derived from layered double hydroxides. *ACS Catal.* **2018**, *8*, 11749−11760.

16. Wei, M.; Zhang, X.; Evans, D. G.; Duan, X.; Li, X. J.; Chen, H. Rh-TPPTS intercalated layered double hydroxides as hydroformylation catalyst. *AIChE J.* **2007**, *53*, 2916−2924.

17. Hubbard, P. J.; Benzie, J. W.; Bakhmutov, V. I.; Blümel, J. Disentangling different modes of mobility for triphenylphosphine oxide adsorbed on alumina. *J. Chem. Phys.* **2020**, *152*, 054718.

18. Xiang, X.; He, W. H.; Xie, L. S.; Li, F. A mild solution chemistry method to synthesize hydrotalcite-supported platinum nanocrystals for selective hydrogenation of cinnamaldehyde in neat water. *Catal. Sci. Technol.* **2013**, *3*, 2819−2827.

Mass spectrometry data for various compounds encountered in this study

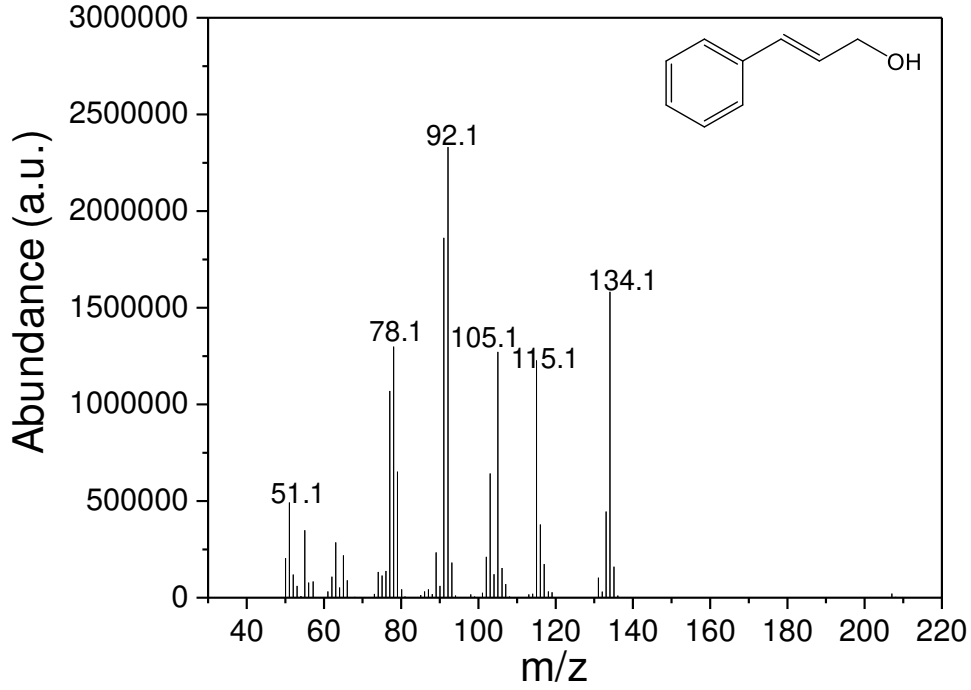

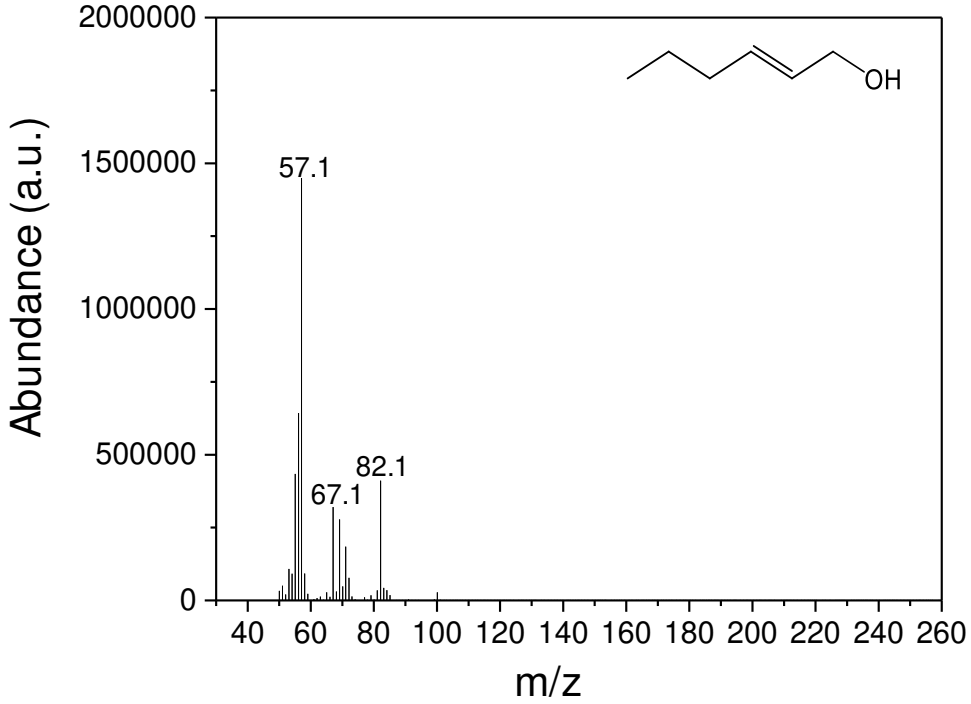

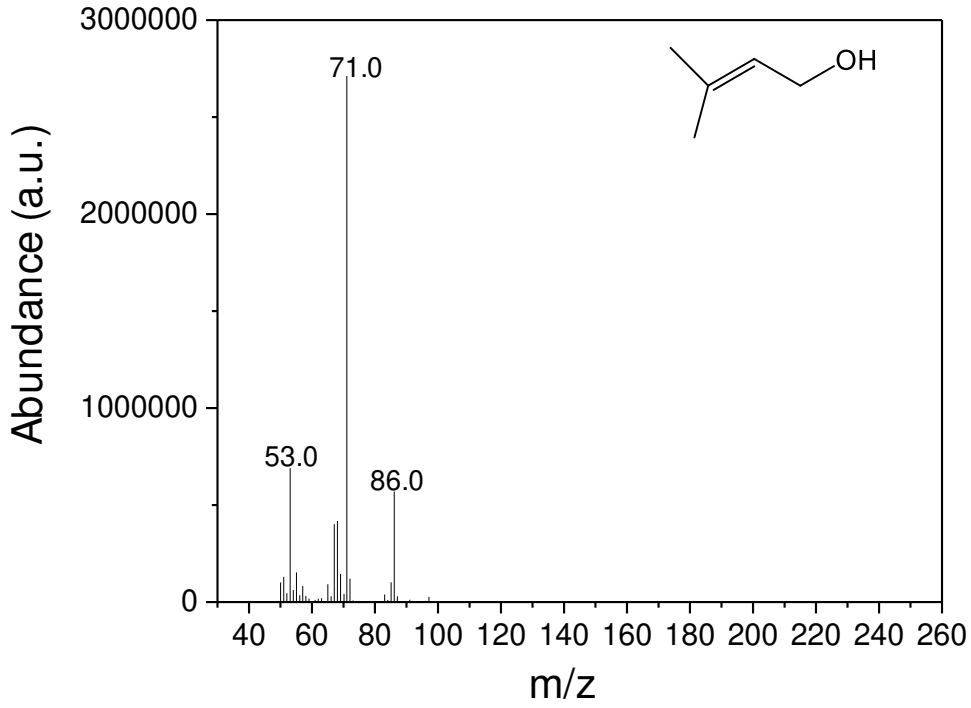
3000000
2000000
1000000
0
Abundance (a.u.)
71.0
53.0
86.0
OH
40 60 80 100 120 140 160 180 200 220 240 260
m/z

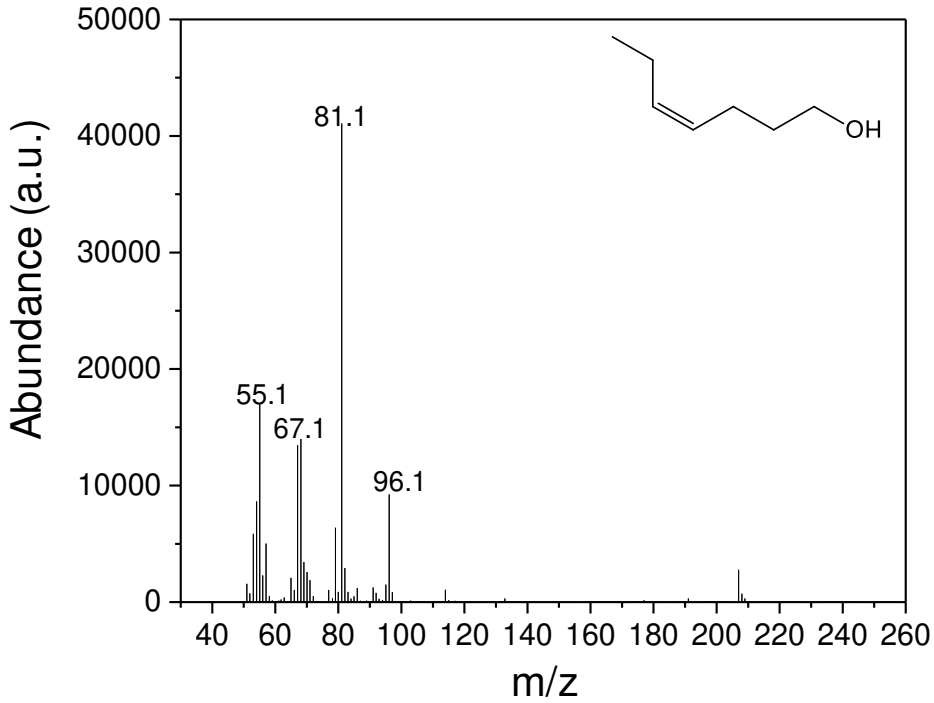
50000
40000
30000
20000
10000
0
Abundance (a.u.)
81.1
55.1
67.1
96.1
OH
40 60 80 100 120 140 160 180 200 220 240 260
m/z

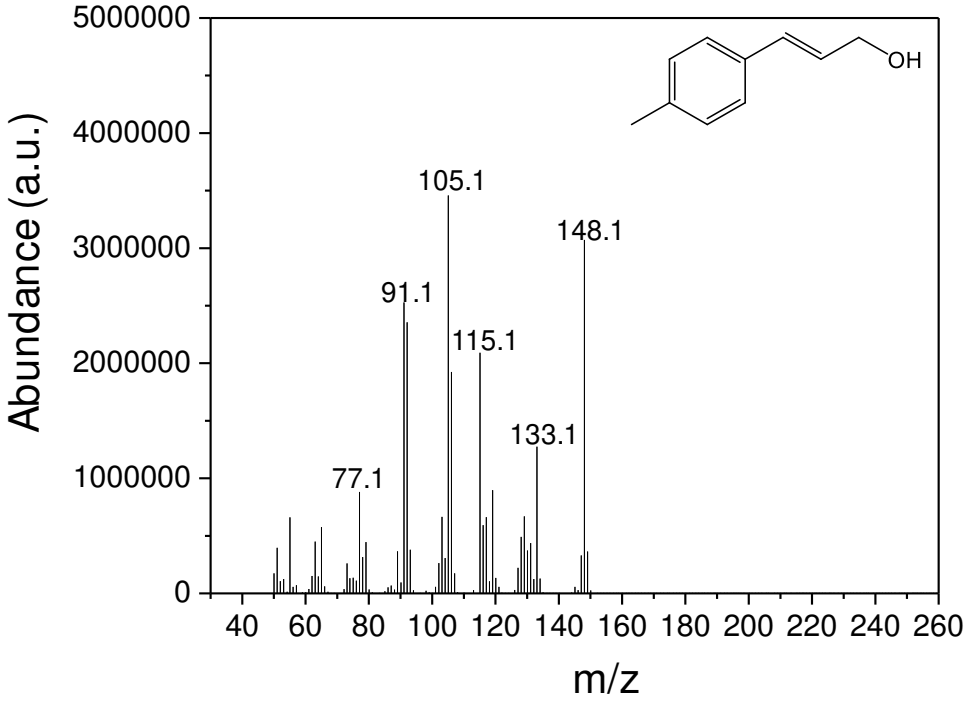
Abundance (a.u.)
5000000
4000000
3000000
2000000
1000000
0
105.1
148.1
91.1
115.1
133.1
77.1
OH
40 60 80 100 120 140 160 180 200 220 240 260
m/z

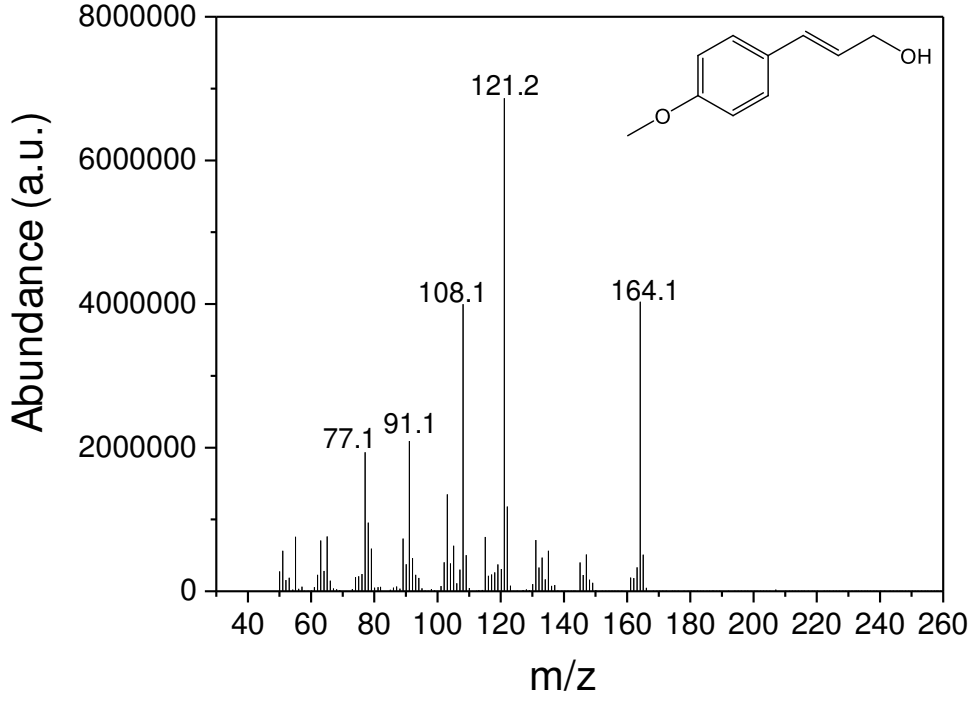
Abundance (a.u.)
8000000
6000000
4000000
2000000
0
121.2
108.1
164.1
77.1
91.1
O
OH
40 60 80 100 120 140 160 180 200 220 240 260
m/z

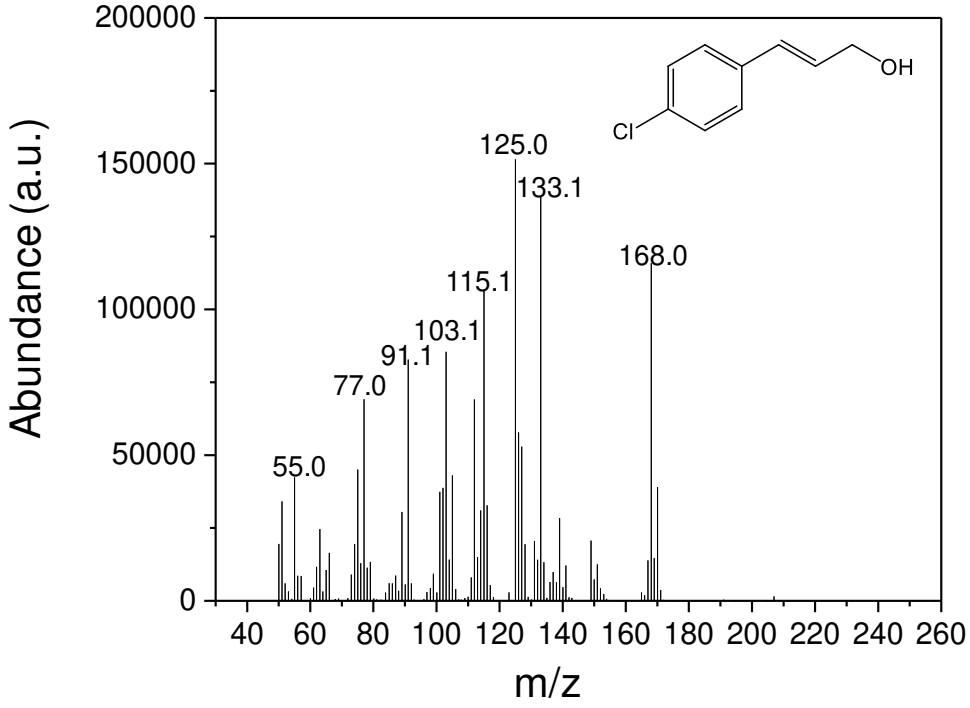
Abundance (a.u.)
m/z
Cl
OH
125.0
133.1
168.0
115.1
103.1
91.1
77.0
55.0

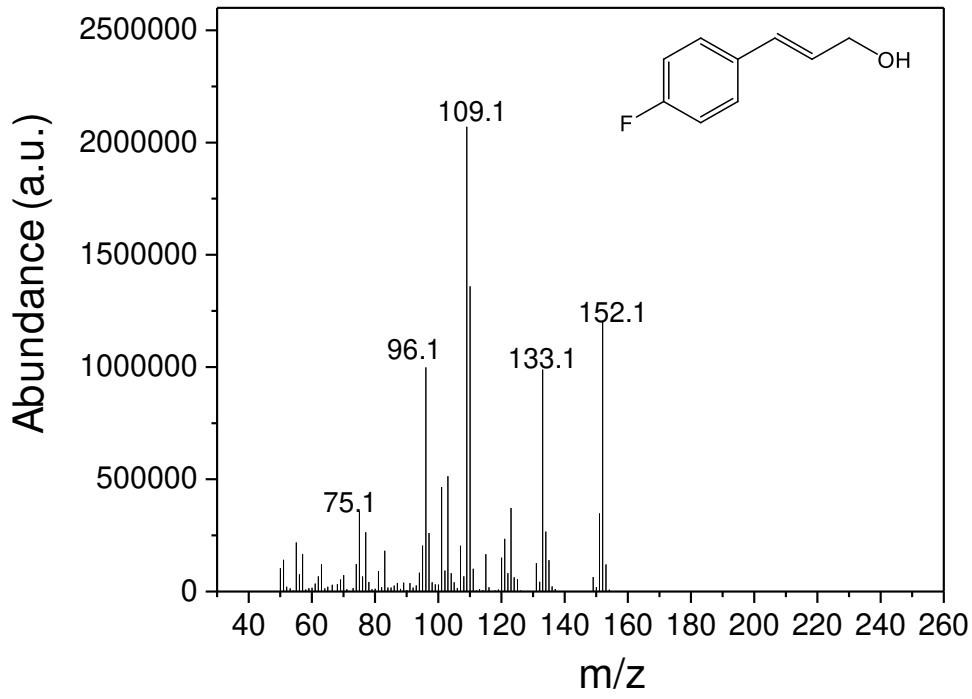
Abundance (a.u.)
m/z
F
OH
109.1
152.1
96.1
133.1
75.1

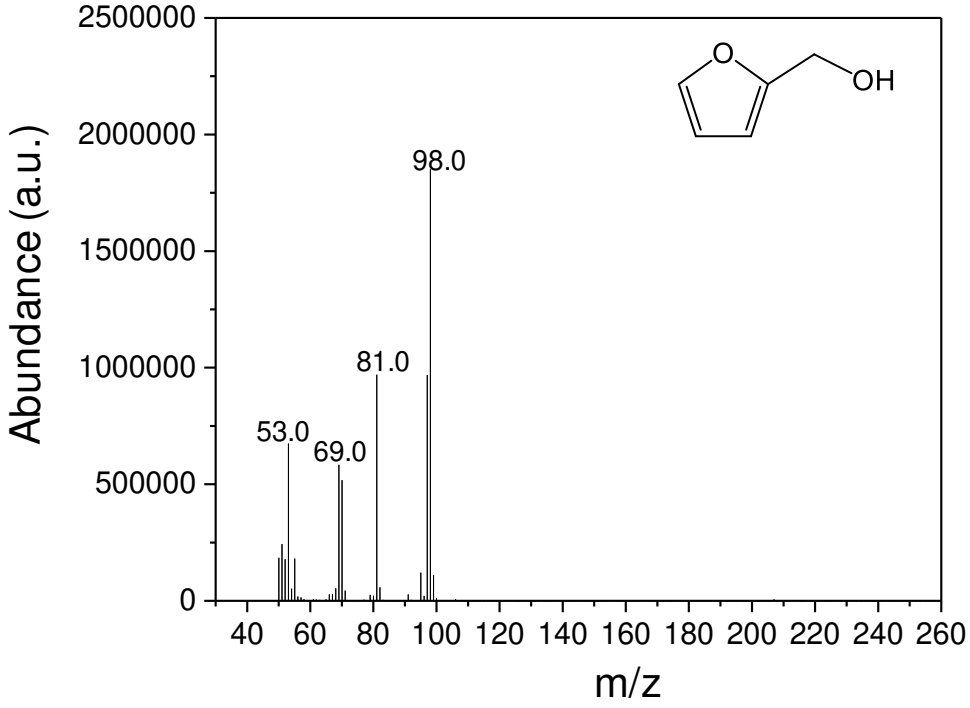
Abundance (a.u.)
m/z
O
OH
98.0
81.0
69.0
53.0

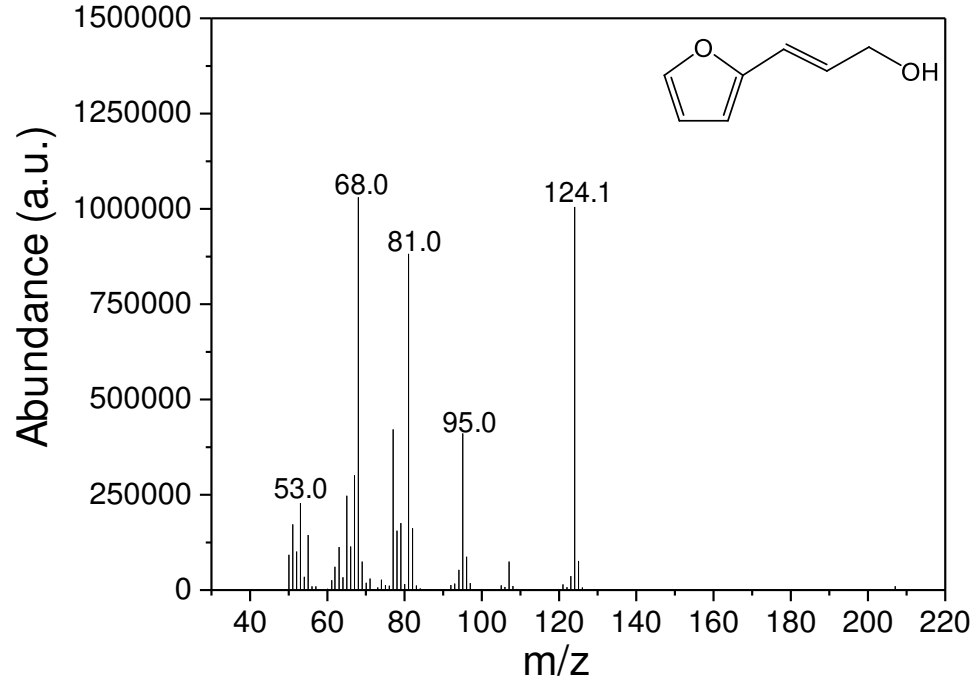
Abundance (a.u.)
m/z
O
OH
68.0
124.1
81.0
95.0
53.0